Dynamics of cortico-subthalamic neuronal patterns during dyskinesia in Parkinson's disease

J. Habets [1,2], T. Merk [1], V. Mathiopoulou [1], R. Lofredi [1,2], T. Binns [1,2,3,4], J. L. Busch [1,2], R. Köhler [1], A. Memarpouri [1], K. Faust [5], P. Krause [1], GH. Schneider [5], WJ. Neumann [1,2,3], P. Tovote [6], A. Kühn [1,2,3,7,8]

1 Movement Disorders and Neuromodulation Unit, Department of Neurology, Charité – Universitätsmedizin Berlin, Germany
2 Berlin Institute of Health (BIH), Berlin, Germany
3 Einstein Center for Neurosciences Berlin, Charité – Universitätsmedizin Berlin, Germany
4 Bernstein Center for Computational Neuroscience, Berlin, Germany
5 Department of Neurosurgery, Charité – Universitätsmedizin Berlin, Germany
6 Institute of Clinical Neurobiology, Universitätsklinikum Würzburg, Germany
7 NeuroCure Clinical Research Centre, Charité – Universitätsmedizin Berlin, Germany
8 Berlin School of Mind and Brain, Humboldt-Universität zu Berlin, Berlin, Germany

Abstract

People with Parkinson's disease suffer from levodopa-induced dyskinesia, adversely to chronic dopaminergic medication. These involuntary movements affect quality of life and are linked to lowered motor inhibition in the cortico-basal-ganglia motor network during hyperdopaminergic states. Several cortical and subcortical spectral biomarkers are associated with dyskinesia, but the oscillatory patterns associated with the behavioral complexity of involuntary movement and voluntary movement suppression that defines dyskinesia, is not studied so far. To elucidate these spatio-temporal dynamics and its behavioral relevance, we studied cortico-subthalamic oscillations in 21 Parkinson's patients during a dyskinesia-provoking experiment. We differentiated between non-dyskinetic and dyskinetic periods, and split data based on a kinematic movement registration, leading to respectively resting states and voluntary movement, and active movement suppression and dyskinetic movement. Elevated theta-activity and attenuated beta-activity was found in the subthalamic nucleus during voluntary movement suppression within dyskinetic periods, while cortico-subthalamic gamma-activity was only elevated during dyskinetic movement presence. Subthalamic spectral changes significantly predicted dyskinesia presence, and the amount of registered movement significantly affected the predictive value of dyskinesia predictions. We propose a dyskinetic macrostate to consist of distinct behavioral microstates of dyskinetic movements versus movement suppression, both associated with distinct oscillations in the cortico-subthalamic motor network.

Main

Dopaminergic replacement therapy is the cornerstone to treat hypokinetic symptoms in Parkinson's disease (PD), but also adversely causes disabling abnormal involuntary movements, defined as levodopa induced dyskinesia (LID) [1–4]. As disease progression continues and requires larger and more frequent dopaminergic intakes, LID occurs in up to 80% of PD patients, impacting quality of life [1,3,5]. LID primarily emerges during moments of dopaminergic peaks and has a fluctuating heterogeneous clinical phenotype of involuntary movements, alternating with episodes of voluntary motor suppression and subjective internal motor restlessness [2]. Typically, LID is treated with either pharmacological interventions that improve levodopa's efficacy and allow dopamine reduction [4] or target specific striatal projecting neurotransmitter-receptors [6]; or with device-aided therapies such as deep brain stimulation (DBS) [5,7–10]. Although overstimulation with DBS can induce dyskinesia [11], DBS generally alleviates LID by allowing a reduction of dopaminergic medication [12] and possibly by a long-term desensitization of dopamine receptors [13].
Current understandings of the pathophysiology of LID hypothesize that a reduced cortical long-term depotentiation alters cortico-striatal synaptic plasticity [14,15]. The impaired synaptic plasticity fails to balance dopaminergic cortico-basal-ganglia excitation and increases the likelihood of movement [16]. On a striatal level, chronic dopamine depletion is hypothesized to cause compensatory structural changes in striatal projection neuron architecture and fast spiking interneurons [17–19]. These compensatory neural changes shift the balance between the canonical direct and indirect motor pathways to restore homeostasis during hypo-dopaminergic periods [17,18,20,21]. Moreover, long term dopaminergic depletion leads to abnormal spiking patterns of SPN neurons with loss of spatial and temporal selectivity [22]. Neural dynamics can partially be restored by dopaminergic treatment, but during hyper-dopaminergic periods, inverse abnormalities in striatal activity pattern with overcompensated reduction in motor inhibition may occur, facilitating LID [22–26]. Since the subthalamic nucleus (STN) is specifically involved in movement planning, execution, and cancellation [27–29], STN DBS can directly modulate physiological motor stopping [30], but also dyskinetic movement [11]. Invasive neurophysiological studies explored biomarkers that represent spectral network oscillations during different motor, cognitive, and emotional states in PD [31]. Subthalamic beta activity has been established as a symptom-specific biomarker for bradykinesia [28], independent of disease [32,33]. Furthermore, cortico-subthalamic gamma activity has been used to decode movement initiation, velocity and stopping [34–36], whereas increased theta band activity has been described in conflicting cognitive tasks during decision making and in impulse control disorders [37,38]. Regarding LID, elevated subthalamic and cortical gamma-band (60 – 90 Hz) activity has been associated with LID presence and severity [39–41], similar to elevated subthalamic theta- and alpha-band (resp. 4 – 8 and 8 – 12 Hz) activity [37], and decreased subthalamic beta-band (13 – 35 Hz) activity [40,42]. The spatiotemporal patterns of oscillations associated with LID so far, have not been differentiated with respect to the highly variable behavioral dynamics of LID [2], i.e. movement execution and movement suppression, and therefore their behavioral relevance within LID remains unclear [31]. This highly variable behavioral pattern within LID, containing both presence and absence of movement execution [2], may modulate neural oscillations by the degree of successful active motor suppression [43]. In this vein, we hypothesize that LID in PD patients consists of distinct behavioral states, with distinct neural oscillations [43], in line with a first rodent study that differentiated between distinct dyskinetic movements in rodents with distinct neural patterns [21].

A recent concept developed to explain integrated systemic, cardio-behavioral states in the context of emotional challenge [44] allows to characterize temporal dynamics of behavioral and physiological changes over variable time-periods [44]. Herein, slow transitions are termed as macrostate changes and contrast fast-changing, momentary microstates, which reflect short-lasting distinct behavioral or

neural patterns.
To gain insight into the behavioral relevance of LID-related biomarkers, we hypothesize that the heterogeneous behavior during dyskinetic periods can be explained by distinguishable neural and behavioral states that differ in spatio-temporal spectral characteristics. First, a prerequisite for LID to occur is the slow transition from the hypodopaminergic OFF state to the hyperdopaminergic ON state in PD, which we consider a macrostate change [44]. On the background of the hyperdopaminergic ON state, fast-changing microstates may occur that lead to the execution of dyskinetic movements. To investigate the hypothesized states-concept, we characterized spectral patterns in invasive subthalamic and cortical neurophysiological recordings from the hypodopaminergic OFF state to the hyperdopaminergic ON state with LID, during the execution of dyskinetic movements and during voluntary movement suppression. The latter behavioral states we defined based on the presence and absence of movement execution during a dyskinetic state. We identified distinct subthalamic theta and beta oscillations associated with the slow-changing dopaminergic periods considered as a macrostate. Fast-changing patterns of cortico-subthalamic gamma oscillations that depend on the presence of dyskinetic movement could be defined as microstate changes. The identification of the behavioral relevance of these spatio-temporal spectral changes during dyskinetic periods will help us to better understand LID's pathophysiology and cortico-subthalamic biomarkers relevant for motor control during LID. This may lead to optimized use of biomarkers for adaptive DBS tailored to clinical demands.

Dyskinetic periods contain moments with and without objectified movement execution

To investigate LID-related spectral patterns, we included twenty-one PD patients implanted with bilateral STN DBS electrodes, of which thirteen received a temporary unilateral electrocorticography (ECoG) electrode (mean age: 61 years, standard deviation (sd): 9.2 years, mean disease duration: 10 years (sd: 4 years)) (see Table S1). All participants performed a dyskinesia-provoking experiment during the interval (two to seven days) between their surgical implantation of DBS-electrodes and its connection to the internal pulse generator [45]. Participants started the experimental protocol in the medication-OFF condition (at least 12 hours of dopamine withdrawal) followed by a supra-threshold dosage of fast-acting levodopa (circa 1.5 morning dose of Madopar LT ®, Roche Pharma). STN and cortical activity were recorded during repetitive rest and unilateral self-paced hand tapping tasks, intermingled with unscripted pauses to avoid fatigue and experiment abortion (see Figure 1 and Fig. S1).
A clinical movement disorders specialist assessed the presence and severity of LID based on video recordings, using the Clinical Dyskinesia Rating Scales (CDRS). [46] The presence of LID was observed in eighteen out of twenty-one participants (86%), of which fifteen had a preoperative history of LID (83%) (see Methods). One participant, that did not develop LID, had a preoperative LID history. The eighteen patients that did develop LID had mean peak dyskinesia severities of 5 CDRS points (sd: 3, range: 2 to 13 CDRS points), out of a maximum of 28 points (the latter corresponds to severe dyskinetic movement in all seven rated body parts).
The distributed repetitions of resting and tapping tasks blocks led to the recording of movement presence and movement absence in both dyskinetic states and non-dyskinetic states (Figure 1). We defined a dyskinetic period as a time interval that starts at the first observed dyskinetic movement and prolongs as long as the patient regularly shows abnormal involuntary movements. Dyskinetic periods will also contain moments of suppression of involuntary movements, usually achieved by active movement suppression with voluntary muscular co-contraction in between dyskinetic movements (Figure 2). Fluctuations in the clinically assessed severity of a dyskinetic period were assessed on a minute level, while the observation of actual movement was objectively assessed on a

sub second level with accelerometer data. Consequently, we differentiated between 1) movement presence during the non-dyskinetic period (i.e. voluntary movements), 2) movement absence during the non-dyskinetic period (i.e. the resting state), 3) movement presence during the dyskinetic period (i.e., execution of both voluntary and involuntary movements, during episodes clinically confirmed as dyskinetic), and 4) movement absence during the dyskinetic period (i.e., epochs of motor suppression, lacking objectified movement execution, within periods clinically confirmed as dyskinetic). This behavioral concept, that dyskinetic periods contain epochs of both movement presence and absence, is essential to assess different neural microstates, i.e. dyskinetic movements, during the hyperdopaminergic macrostate characterized by a dyskinetic period.

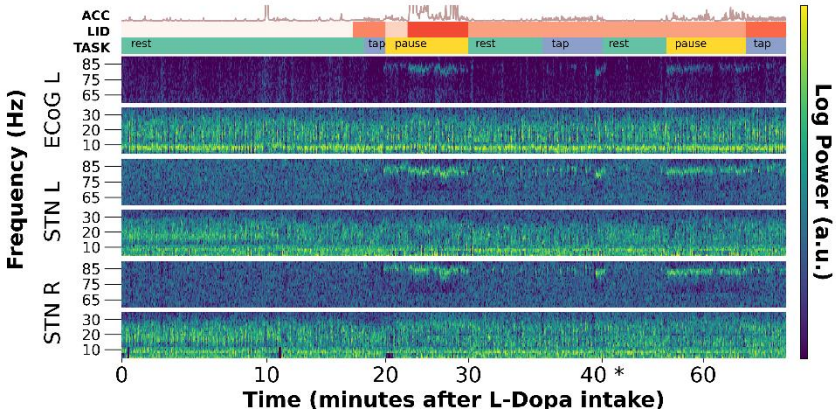

Figure 1: Single subject example of spectral changes and behavioral heterogeneity during dyskinetic periods. Neural, behavioral, and clinical data from one subject is shown. The first upper row (ACC) represents the participant's activity, recorded via bilateral accelerometers placed on the index-fingers. The line shows the average of the z-scored root mean squares of both accelerometers. The second upper row (LID) represents the clinically assessed dyskinesia presence and severity (defined as sum CDRS) over time. The first white part represents the non-dyskinetic period. A dyskinetic period is represented by different shades of orange, where darker orange represents more severe LID. LID occurred bilateral in this subject, with more severe dyskinetic movements in the right body side compared to the left. The third upper row represents the task performed (TASK) during the experiment, in which *rest* contained seated rest*, tap* contained a seated self-paced, unilateral hand-tapping task, and *pause* contained an unscripted pause for the participant to prevent fatigue.
The three neural time-frequency plots represent spectral unilateral cortical (ECoG) and bilateral subthalamic (STN) activity. Note the decrease in beta activity bilaterally in the STN at about 10 minutes after levodopa intake and during LID, and irregular gamma synchronization during LID, mostly in the presence of movement.
*: The recording was interrupted around minute 45 for a toilet break and the x-axis is adjusted accordingly.
ECoG: electrocorticography, Hz: Hertz, L-Dopa: levodopa, LID: levodopa induced dyskinesia, STN: subthalamic nucleus.

Multi-frequency cortico-subthalamic oscillatory patterns reflect dopamine-induced dyskinetic macrostate changes

Time-frequency analyses of the subthalamic and cortical recordings demonstrated changes in spectral patterns with levodopa-intake in different frequency ranges of interest (see the exemplary case in Figure 1). Spectral activity was calculated using an unbiased data-dimensionality reduction method (spatio-spectral decomposition) on the multi-channel recordings and resulted in single time-frequency data per recording site [47]. These data are optimized independently regarding signal-to-noise ratios per frequency band of interest (theta, beta, and gamma band; see Methods).
We hypothesized that distinct neural oscillatory patterns occur during hyperdopaminergic ON periods and correlate with the severity of dyskinetic periods. To this end, we first descriptively compared local STN and cortical changes occurring with the transition from OFF to ON dopaminergic periods and during different LID severity grades. All neural data from the rest and tap task were included, without specifying movement presence and absence. CDRS raters were blinded for neurophysiological results and scores were categorized into mild (less than 4 points), moderate (4 to 8 points), and severe LID (8 or more points) [46]. Power spectral densities calculated over 10-second epochs showed an increase in subthalamic theta activity that occurred during the dopaminergic ON period without LID and gradually increased with LID-severity, whereas subthalamic low-beta activity showed a gradual decrease. Similarly, this low-beta decrease extended the low-beta decrease observed in both all non-dyskinetic periods as well as in ON-periods periods without LID after 30 minutes post-levodopa-intake (Figure 2, upper row). A large increase in narrow band gamma activity was observed in both subthalamic and cortical data predominantly during the dyskinetic periods but did not show a strong scaling effect with LID severity. Additionally, we calculated squared coherences in the same epochs to investigate how LID affects spectral connectivity between the two STNs and between the cortex and the ipsilateral STN. Inter-subthalamic coherence showed small and variable increases in theta-coherence and decreases in beta-coherence during the dyskinetic period but no obvious scaling effect (Figure 2, lower left). Gamma-activity was coherent between the cortex and the ipsilateral STN only in the two patients with severe LID.

Together, these spectral changes represent distinct neural patterns that represent medication induced macrostate changes: importantly, we describe the differences not only for the dopaminergic transition to the ON medication state without LID, but the dyskinetic state demonstrates a further spectral modulation.

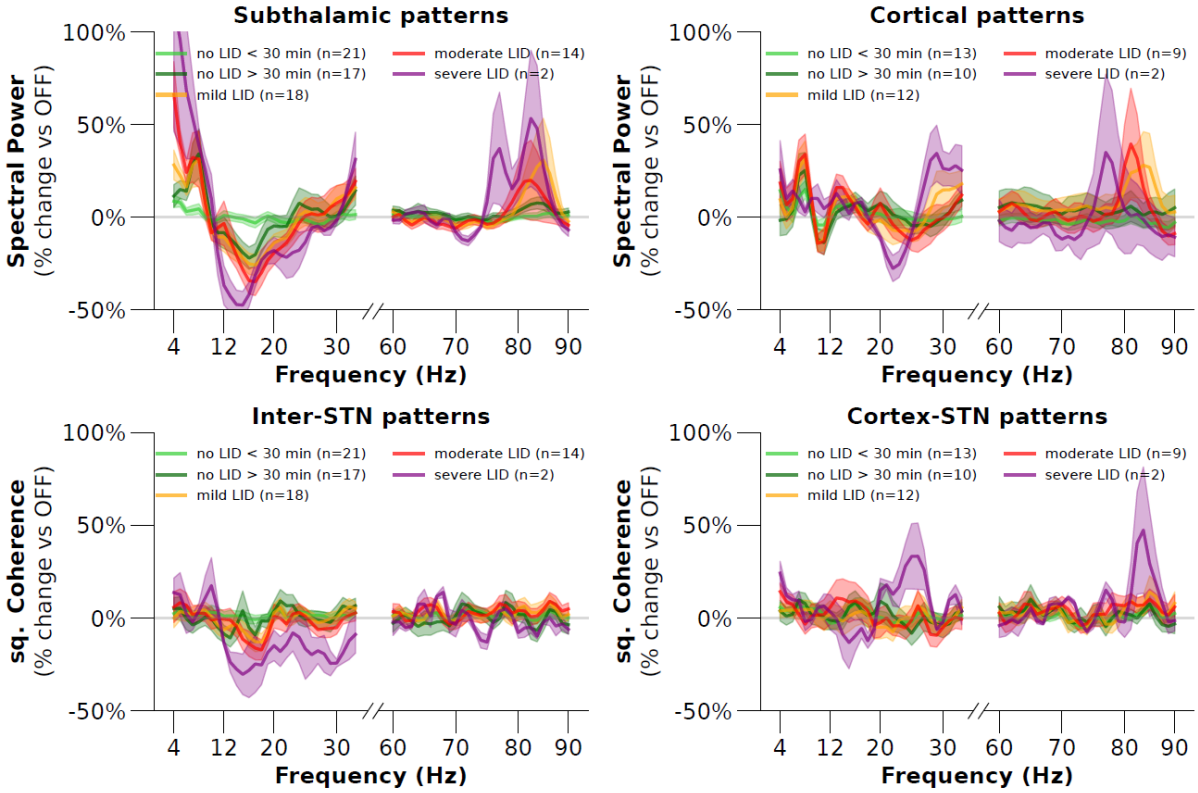

Figure 2: Spectral subthalamic and cortical patterns change during dyskinetic periods depending on dyskinesia severity.

All four panels show the changes in spectral patterns as percentage changes relative to the dopaminergic OFF condition at rest up to five minutes after levodopa-intake. Three grades of dyskinesia severity are visualized: mild LID in yellow (1 to 3 CDRS points), moderate in red (4 to 7 CDRS points), and severe in purple (8 or more CDRS points). The OFF and ON conditions are visualized in light and dark green. The numbers in the legend represent the number of subjects that contributed neural data to a category.

The upper row shows power spectral densities of subthalamic nucleus (STN) (upper left) and cortical (upper right) recordings. Note the increase in STN theta and decrease in beta activity that scale with severity of dyskinesia, the scaling effect is less prominent for gamma synchronization with dyskinesia in STN and cortex. Spectral powers are calculated using Welch's method per ten-second windows and the panels show means and standard error of the means for individual averages per category. Spectral powers of bilateral STNs are averaged per window. The lower row shows squared coherences between the two STNs (lower left) and between the cortex and the ipsilateral STN (lower right) and demonstrates a decrease in beta coherence and increase in cortico-STN gamma coherence during LID, with less prominent changes. Squared coherence spectra are calculated in ten-second epochs using Welch's method. All lines were smoothed with a 3 Hz bin for visualization.

Hz: Hertz, LID: levodopa-induced dyskinesia, OFF: medication Off, STN: subthalamic nucleus, sq.: squared.

Subthalamic theta- and beta-oscillations are associated with movement absence in between dyskinetic movements

The observed changes in oscillatory cortical and subcortical neuronal pattern have been associated with LID presence in prior studies [37,40,42]. To explore the behavioral relevance of these long-lasting, dopamine-dependent macrostate changes (Figure 2) and their interaction with short-lasting movements, we split the neural data based on the presence and absence of movement. We first

229 defined dyskinetic versus non-dyskinetic periods based on the clinical expert assessments of video
230 recordings of the full protocol. Dyskinetic periods were identified as behavioral states that lasted at
231 least several minutes, and did not change on a (sub)-second resolution. Within these periods (i.e.,
232 macrostates), movement presence and absence were defined using bilateral index-finger worn
233 accelerometer data (TMSi Saga®, TMSi International, Oldenzaal, The Netherlands). Movement
234 absence was verified by video protocol to exclude movements on other parts of the body. Movement
235 start- and end-points were defined on a sub-second resolution based on a thresholding procedure
236 and led to epochs of movement presence and absence (i.e., microstates). Combining the sub second
237 movement detection with the clinical assessments of LID presence, resulted in the categorization of
238 all neurophysiological data into the four mentioned behavioral categories, i.e. movement presence
239 versus absence, and dyskinetic versus non-dyskinetic periods (Figure 3). We did not differentiate
240 between voluntary and involuntary movements during dyskinetic period, since these two concepts
241 are not reliably distinguishable. During dyskinetic periods, patients often try to mask involuntary
242 movements with a voluntary movement, and voluntary movements vice versa often evolve into or
243 provoke involuntary movements. All data were merged within the respective clinically relevant
244 behavioral categories to identify the distinct neural pattern and its modulation during microstates of
245 movement presence. Additionally, we defined an ON condition without LID, i.e., time points after 30
246 minutes post-levodopa-intake without LID (n = 15), to allow comparison of dyskinetic effects versus
247 non-dyskinetic dopaminergic medication effects. Neural data were analyzed per recording source,
248 i.e. per STN or ECoG electrode, using the first component of an un-biased spatial spectral
249 decomposition method to reduce the data-dimensionality while optimizing the signal-to-noise ratio
250 [47]. Neural data were merged within their respective microstate clusters for LID- and movement-
251 presence and underwent time-frequency decompositions allowing for spectral comparisons per
252 canonical frequency band of interest (Figure 4) (see Methods).

253

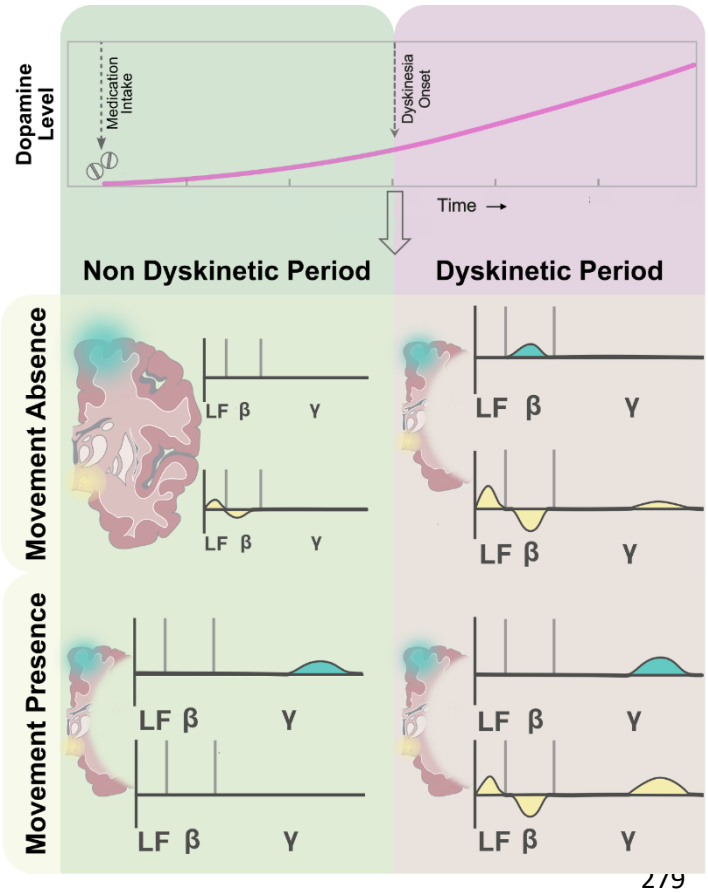

Figure 3: Schematic overview of dyskinesia-related spectral patterns during the presence and absence of executed dyskinetic movement. This schematic visualization illustrates that the clinical manifestation of both dyskinetic and non-dyskinetic periods contain moments of movement absence and presence. The upper line plot visualizes the rising dopamine blood-levels after medication intake. In the hyperdopaminergic state, dyskinetic periods occur when levodopa-levels are elevated sufficiently. Green PSD panels (left) represent non-dyskinetic periods, classified as a total Clinical Dyskinesia Rating Scale of zero at all time points. Purple PSD panels (right) represent dyskinetic periods. Dyskinetic periods fluctuate slowly over time with typically durations in a minute to half hour range, depending on individual disease progression, pharmacodynamics, and levodopa dosage. Movement presence and absence fluctuate more frequently and faster, on a seconds-resolution. Green PSDs represent cortical recordings and yellow PSDs represent subthalamic recordings. Spectral bands are shown on the x-axes: LF: low-frequency activity (theta and alpha, 4 – 12 Hz), beta activity (13 – 35 Hz), gamma activity (60 – 90 Hz). The y-axes represent the magnitude of spectral powers. LF: low-frequency, min: minutes. Spectral elevations and attenuations in this graphic are based on the spectral results, but the heights of the peaks are relative and not absolute.

Spectral power densities and squared coherences were compared between the behavioral categories, within every frequency band of interest (Figure 4 and 5). First, we describe changes in neuronal network activity that occur **within dyskinetic periods in the absence of movement execution**. *Subthalamic theta and alpha band increase and low-beta band reduction* were significantly larger in the dyskinetic period compared to the non-dyskinetic periods (resp. coefficients of linear mixed effect models (lmm-coeff.) 0.17, p=0.0001, 0.11, p<0.0001 and -0.14, p<0.0001) (Figure 4B). Importantly, these LID-related changes extended changes occurring during the ON without LID condition. When statistically testing the dyskinetic period versus the ON condition, subthalamic low-beta decrease and theta and alpha increase remained significant (resp. lmm-coeff.: -0.07, p<0.0001; 0.09, p<0.0001; and 0.09, p<0.0001). A significant low-beta reduction also occurred in the ON versus the OFF condition, this was however a smaller effect size than the dyskinetic-related changes (lmm-coeff. -0.11, p>0.0001). Theta and alpha increases did not differ between ON without LID and OFF conditions (lmm-coeff 0.10, p=0.20, 0.08, p=0.03).
Both individual peak gamma-activity, as well as broad-gamma activity, showed a small but significant increase during dyskinetic periods compared to all non-dyskinetic periods (lmm-coeff. resp: 0.03, p<0.0001; 0.03, p<0.0001). However, these increases did not remain significant when comparing the dyskinetic periods with the non-dyskinetic ON condition (lmm. coeffs.: 0.00, p=.98 and -0.01, p=0.04)

but were significant in comparison with the OFF conditions (resp. lmm-coeff.: 0.03, p=0.001; 0.03, p<0.0001).

Regarding cortical power modulation during dyskinetic periods in movement absence, we observed small but significant low-beta increase (lmm-coeff. 0.04, p=0.0015) and gamma-activity decreases (peak- and broad-gamma resp. lmm-coeff. -0.02 and -0.08, p<0.0001 and p<0.0001) (Figure 4, lower panels). These cortical changes did not remain significant when comparing the dyskinetic periods with the non-dyskinetic ON condition (resp. lmm.-coeffs.: 0.04, p=0.03; 0.00, p=0.87; and -0.01, p=0.28). We cannot exclude that these small changes are overemphasized following the normalization influenced by the changes during movement presence that are in higher magnitudes of order.

In line with the observed STN power patterns, also *inter-subthalamic coherences significantly increased in the theta band and decreased in the low-beta band* in the absence of movement during dyskinetic periods compared to non-dyskinetic periods (Figure 5, upper row, resp. lmm-coeff. 0.35, p<0.0001 and -0.08, p<0.0001). This LID-associated theta and low-beta modulation remained significant compared to ON periods without LID (lmm.-coeffs.: 0.36, p<0.001 and -.08, p<0.001) but no difference occurred between ON and OFF conditions suggesting that the theta- and beta-coherence modulation is specific to the dyskinetic periods (lmm-coeff. resp. 0.00, p=0.935 and 0.00, p=0.855). Inter-subthalamic peak-gamma showed a minor but significant difference between dyskinetic and non-dyskinetic periods (lmm-coeff. 0.02, p=0.0004), whereas alpha and broad-gamma bands did not differ significantly (lmm-coeff. resp. -0.01, p=0.74; 0.01, p=0.08). Cortico-subthalamic theta- and beta-coherences did not change significantly between dyskinetic and non-dyskinetic periods in the absence of movement (lmm-coeff. resp. 0.06, p=0.02; and 0.01, p=0.79), whereas alpha activity showed a trend for an increase (lmm-coeff. 0.08, p=0.001). C*ortico-subthalamic gamma coherences in peak- and broad-frequencies* showed a small but significant increases in the dyskinetic periods compared to non-dyskinetic periods (Figure 5 lower row, lmm-coeff. resp. 0.04, p<0.0001, and 0.06, p<0.0001) that remained increased compared to ON conditions (lmm-coeffs. resp. 0.04, p<0.001, and 0.06, p<0.001).

Taking together, these results demonstrate that movement absence during dyskinetic periods is characterized by increased subthalamic theta and alpha activity and decreased beta activity that significantly differ from the non-dyskinetic ON condition and thus may represent a distinct macrostate (Figures 4 and 5). In contrast, the small STN gamma power increase was more related to a general dopamine ON condition and only the increase in cortico-STN coherence was associated with the dyskinetic period.

Dyskinetic movements are characterized by increased gamma activity in STN and cortex

To investigate whether **movement presence during dyskinetic periods** can be identified and objectified as a **microstate** in neural recordings, we isolated movements during dyskinetic periods based on accelerometer data. To ensure that network pattern changes during movement presence are specific for dyskinetic movements, we compared them with movement presence during non-dyskinetic periods, extracted from the voluntary tapping task. Subthalamic theta and alpha activity showed a trend for an increase during dyskinetic movement compared to all recorded non-dyskinetic movement (Figure 4 right upper panel, lmm-coeff. resp. 0.16, p=0.002 and 0.06, p=0.035). Low-beta activity decreased significantly during dyskinetic movement presence compared to non-dyskinetic movement presence (lmm-coeff. -0.15, p<0.001). Subthalamic broad-gamma activity, but not peak-

gamma activity, increased significantly during dyskinetic movement compared to non-dyskinetic voluntary movements (resp. lmm-coeff. 0.03, p=0.0001; 0.01, p=0.044). Similarly, cortical broad-gamma activity significantly increased during dyskinetic movement compared to non-dyskinetic movement (lmm-coeff. 0.13, 0.0012, Figure 4, upper right panel). Cortical theta, beta, and peak-gamma activity did not show significant changes during dyskinetic versus non-dyskinetic movements. To examine that these changes are specific for movement during dyskinetic periods, instead of merely associated with movement during the dopaminergic ON state, we isolated all voluntary movements that occurred in non-dyskinetic states more than 30 minutes after levodopa-intake (n = 9 subjects). In line with the assumption that gamma activity codes motor parameter, peak-gamma activity showed a significant increase during dyskinetic movement compared to ON medication movement (lmm-coeff. 0.08, p=0.011), whereas theta, low-beta, and broad-gamma did not (lmm-coeffs. resp. 0.03, -0.05, and 0.0, p all > 0.12). Due to limited data availability of ON medication movement data, we only compared these main 4 frequency bands and could not assess cortical spectral changes.

Inter-subthalamic coherence during dyskinetic periods showed similar changes during movement presence as mentioned during movement absence. Theta coherence increased and low-beta coherence decreased during movement in dyskinetic periods, although only the latter reached statistical significance (lmm-coeff. resp. 0.20, p=0.006 and -0.13, p<0.001). Inter-subthalamic gamma coherence did not change significantly. Although larger cortico-subthalamic gamma coherence was observed during dyskinetic movements, none of the changes reached statistical significance, possibly due to high inter-individual variance (Figure 5, lower right).

In order to characterize the movement-related microstate changes during dyskinesia, we lastly compared the neural patterns during movement absence and presence within the dyskinetic period. Here, we found both subthalamic and cortical peak-gamma to be significantly higher during dyskinetic movement presence compared to dyskinetic movement absence (resp. lmm-coeff. 0.08, p<0.0001; and 0.24, p<0.0001). Also, cortical broad-gamma activity showed a significant increase during dyskinetic movement presence compared to dyskinetic movement absence (lmm-coeff. 0.18, p<0.001). Subthalamic broad-gamma activity however, showed a small but significant decrease in dyskinetic movement presence compared to dyskinetic movement absence (lmm-coeff. -0.02, p=0.0001). We argue that this small coefficient in the opposite direction as hypothesized, can be explained by the parallel increases in broad gamma during both dyskinetic movement absence and presence compared to non-dyskinetic periods. Modulations in cortical theta were significantly higher during dyskinetic movement presence versus absence (lmm-coeff. 0.3, p<0.001), whereas subthalamic theta and both subthalamic and cortical beta activity did not differ significantly (lmm-coeff. resp. 0.02, p=0.04; -0.01, p=0.20; and 0.06, p=0.03).

Together, when comparing movement presence with movement absence, both during dyskinetic periods, dyskinetic movement is characterized by peak-gamma increases in the STN and the cortex, and broad-gamma increases in the cortex. Subthalamic broad-gamma already shows an increase during dyskinetic periods in movement absence, which even slightly extends the increase during movement presence. These findings demonstrate that the hypothesized cortical gamma activity related to LID is specific to movement presence during LID, and that increased activity in cortical gamma as well as subthalamic peak-gamma extend gamma modulation during non-dyskinetic, dopaminergic-ON movement presence.

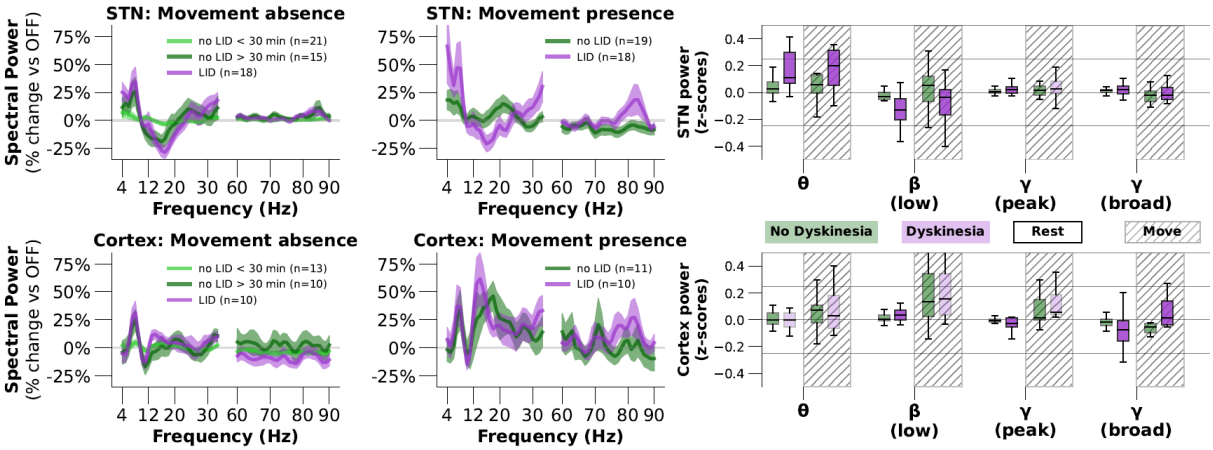

Figure 4: Movement modulates local subthalamic and cortical patterns during dyskinetic periods

Overall, theta increases and beta decreases in the STN were significant larger during dyskinetic states in both movement absence and presence compared to non-dyskinetic states. Increased gamma activity in the STN during dyskinetic states was mainly observed during the dyskinetic microstates with movement presence. The left four panels show power spectral densities (PSD) of subthalamic recordings (upper row) and cortical recordings (lower row). The upper and lower left PSD-panels show microstates of movement absence, upper and lower right PSD-panels show microstates of movement presence. Movement presence was assessed based on accelerometer-data according to a thresholding procedure. All green lines represent the mean over all individual average-PSDs during non-dyskinetic periods, whereas purple lines represent the dyskinetic periods. Only during movement absence, we differentiated the OFF and ON conditions within non-dyskinetic periods with sufficient sample sizes (light and dark green line respectively). Shadings show the standard error of the mean of the individual averages and legends show the number of included subjects per category.
The two boxplots in the right panel visualize the mean spectral power values focused on the main spectral bands of interest (theta, low-beta, and gamma), originating from the same data as shown in the four PSD panels. For visualization purposes we decided to show these 4 main frequency bands of interest. Green and purple boxes represent respectively non-dyskinetic and dyskinetic periods. The diagonally striped backgrounds indicate movement presence data, whereas movement absence data do not have a background shading. Statistically significant differences between non-dyskinetic and dyskinetic periods, either within movement absence data or within movement presence data, are visualized as full-colored purple boxes. Transparent purple boxes indicate no significant difference compared to a neighboring green box. Alpha-values for significance testing are 0.01 and corrected for six multiple comparison (alpha is 0.0016).
Hz: Hertz, LID: levodopa induced dyskinesia, min: minutes after levodopa-intake, n: number of unique subjects included in category, STN: subthalamic nucleus. Spectral band symbols: θ: theta (4 – 8 Hz), α: alpha (8 – 12 Hz, not shown), β-low: low-beta (12 – 20 Hz), β-high: high-beta (20 – 30 Hz, not shown), γ-peak: individual gamma peak (5 Hz bin around peak between 60 and 90 Hz), and γ-broad: broad-gamma (60 – 90 Hz).

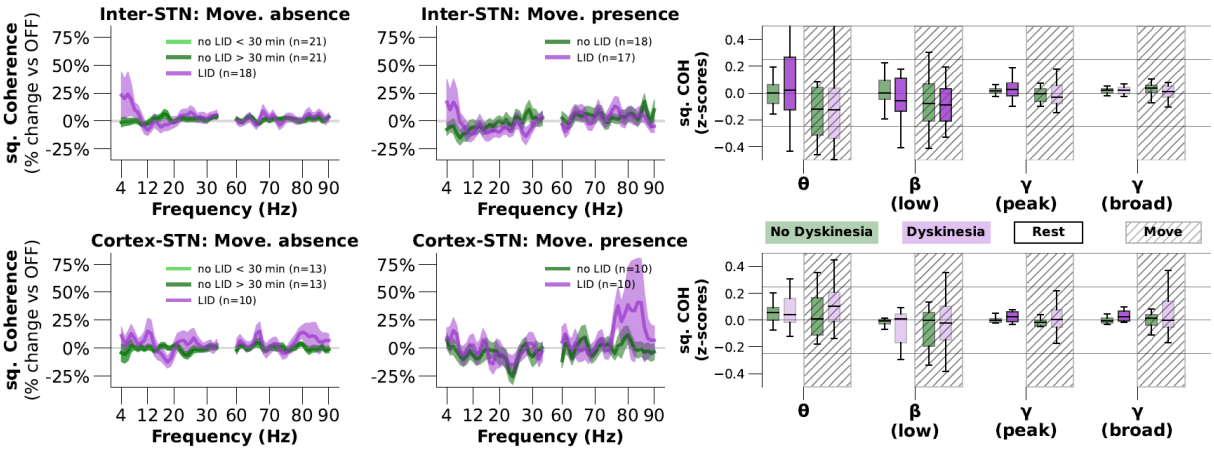

Figure 5: Cortico-subthalamic connectivity changes during dyskinetic periods

The left four panels show squared coherences between bilateral subthalamic recordings (upper row) and ipsilateral cortico-subthalamic recordings (lower row). The upper and lower left coherence-panels show movement absence, the upper and lower right coherence-panels show microstates of movement presence. All green lines represent the mean over all individual average- coherences during non-dyskinetic periods, whereas purple lines represent the dyskinetic periods. Only during movement absence, we could differentiate the OFF and ON conditions within non-dyskinetic periods with sufficient sample sizes (light and dark green lines, respectively). Shadings show the standard error of the mean of the individual averages and legends show the number of included subjects per category. Squared coherences are calculated based on one-second epochs using power spectral densities (psd) and cross spectral densities (csd) by Welch's method ($|\text{csd(source-1 and source-2)}|^2 / (\text{psd(source-1)} * \text{psd(source-2)})$, see Methods).

The two boxplots in the right panel visualizes the mean spectral power values focused on the main spectral bands of interest (theta, low-beta, and gamma), originating from the same data as shown in the four coherence panels. Green and purple boxes represent respectively non-dyskinetic and dyskinetic periods. The diagonally striped backgrounds indicate movement presence data, whereas movement absence data do not have a background shading. Statistically significant differences between non-dyskinetic and dyskinetic periods, either within movement absence data or within movement presence data, are visualized as full-colored purple boxes. Transparent purple boxes indicate no significant difference between a neighboring green box.Alpha-values for significance testing are 0.01 and corrected for six multiple comparison (alpha is 0.0016).

Hz: Hertz, LID: levodopa induced dyskinesia, min: minutes after levodopa-intake, n: number of unique subjects included in category, STN: subthalamic nucleus. Spectral band symbols: θ: theta (4 – 8 Hz), α: alpha (8 – 12 Hz), β-low: low-beta (12 – 20 Hz), β-high: high-beta (20 – 30 Hz), γ-peak: individual gamma peak (5 Hz bin around peak between 60 and 90 Hz), and γ-broad: broad-gamma (60 – 90 Hz). Coherence plots on the left were smoothed with a 3 Hz bin for visualization.

Dyskinetic patterns lateralize contralateral in the cortex but spread bilateral in the STN

So far, we have observed relevant changes in spectral oscillatory activities during dyskinetic periods in both the absence and presence of movement (Table 1 and Figures 4-5). To better understand the pathophysiological role of these LID-related changes within the cortico-basal-ganglia-motor network, we investigated their laterality with respect to clinically observed LID. For this sub analysis, we selected all dyskinetic periods of unilateral LID. Unilateral LID was defined as a sum CDRS of 1 or higher for one body side, while the sum of the other body side remained 0 CDRS points. Typically, unilateral LID marks the beginning of a dyskinetic period and often occurs at the more affected side of the body. Sixteen subjects experienced unilateral LID, of which eleven received a unilateral ECoG-electrode. This led to cortical recordings from five ipsilateral and six contralateral hemispheres with respect to the dyskinetic body side and subthalamic recordings from sixteen bilateral hemispheres. Ten-second epochs during unilateral dyskinetic periods containing both movement presence and

absence were selected to ensure a sufficient sample size.
STN recordings showed bilateral theta and gamma power elevation and beta power reduction during unilateral LID (Figure 6, left panel). In contrast, cortical recordings only showed narrow gamma activity in hemispheres contralateral to the dyskinetic body side (Figure 6, right panel). Cortical recordings ipsilateral to the dyskinetic body side displayed an elevated mean gamma activity without a distinct peak. Modulation of cortical theta and beta activity did not show a consistent pattern. We suggest this to be due to the limited number of included subjects per group and the lack of movement selection. The observed results suggest that the specific subthalamic oscillatory activities during dyskinetic periods occur bilateral, whereas cortical LID-related oscillatory activity occurs only contralateral to the dyskinetic body side. Based on these findings, we excluded all cortical recordings during unilateral dyskinetic periods, originating from the hemisphere ipsilateral to the unilateral dyskinetic body side for further analyses.

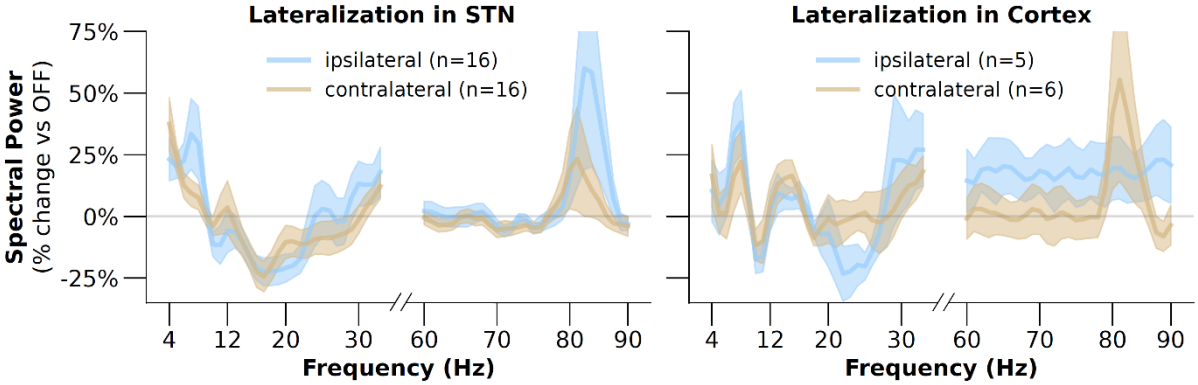

Figure 6: Lateralization of spectral patterns during unilateral dyskinetic periods
Percentage-changes in power spectral densities during clinical observations of unilateral dyskinetic periods are shown in subthalamic nucleus (STN) data (left panel) and cortical data (right panel). Subthalamic theta and gamma elevations and beta-reductions occur in both contra- and ipsilateral data, while cortical gamma elevations only occur in the contralateral hemisphere opposed to the dyskinetic body side. All data result from Welch-transformations per ten-second epochs, without objectified movement selection. All percentage-changes are relative to the medication "OFF" state, defined as all non-dyskinetic-moments within the first five minutes after levodopa-intake, in the absence of movement, objectified with bilateral index-finger accelerometers. The blue lines represent spectral power changes in the hemispheres ipsilateral to the dyskinetic body side; sand-color lines represent spectral power changes in the hemispheres contralateral to the dyskinetic body side. Due to the presence of bilateral STN-electrodes in all sixteen subjects with unilateral dyskinetic periods, and only unilateral ECoG-electrodes in the eleven subjects with unilateral dyskinetic periods and an ECoG-electrode, sample sizes differ per visualized group. We smoothed all lines with a 3 Hz bin for visualization.
Hz: Hertz, LID: levodopa-induced dyskinesia, OFF: medication Off, STN: subthalamic nucleus.

Theta- and gamma-increase and beta-decrease scale with dyskinesia severity

We demonstrated how neuronal patterns during dyskinetic periods differ regarding the absence or presence of movement. In this sub-analysis, we investigated the dependence of LID-related oscillatory activity on the severity of the dyskinetic periods. For this, we included the spectral powers and coherences originating from all three experimental tasks (i.e., resting states, tapping, and unscripted pauses, Figure 1) and quantified movement presence per ten-second epoch. Movement was quantified as mean root mean squares (ACC-RMS) of bilateral accelerometer data and ACC-RMS values were individually z-scored. LID severities were expressed as total sum CDRS scores.

Subthalamic theta-, beta-, and gamma-activity changed gradually with increasing LID severity (horizontal gradients in Figure 7, left column). The gradual theta increases and beta decreases occurred over the whole range of movement presence, showing no clear gradient related to the amount of movement presence (Figure 7, left, upper two panels). In contrast, gamma increases during more severe LID did show a gradient depending on movement presence. During low movement presence (i.e., ACC-RMS below 0) gamma activity only increased at high LID severities (i.e., 8 CDRS points), whereas gamma activity during higher movement presence (i.e., ACC-RMS above 0) showed increases already at lower LID severities (i.e., 4 CDRS points). These findings confirm that the LID-severity-related subthalamic gamma elevations are movement dependent whereas subthalamic theta and beta attenuations are movement independent (Figure 7, left lowest panel).

Cortical spectral patterns demonstrated similar but smaller associations with the severity of the dyskinetic period, as expected based on the cortical patterns during the dyskinetic period regardless of LID severity (Figure 2 and 4). Cortical theta activity increased and beta activity decreased gradually with increasing LID severity, without difference between the amounts of movement presence (Figure 7, right upper panel). Similar to the subthalamic findings, elevations in cortical gamma activity were only seen in mild dyskinetic periods (i.e., up to 4 CDRS points) with higher movement presence (i.e., ACC-RMS above 0). Cortical gamma in more severe dyskinetic periods (i.e., more than 4 CDS points) occurred also with less movement presence (Figure 7, right lower panel).

The observed inter-subthalamic coherences demonstrated similar patterns as the local subthalamic spectral powers (Figure S3, left column). Inter-subthalamic theta- and gamma-coherences showed a gradual increase with increasing severity of the dyskinetic period. In addition, inter-subthalamic gamma-coherence showed the strongest dependence on the amount of objectified movement presence. The coherences between the cortex and the ipsilateral STN were most clearly influenced by both the severity of dyskinetic periods, as well as the amount of movement presence in the gamma-range (Figure S3, right panels).

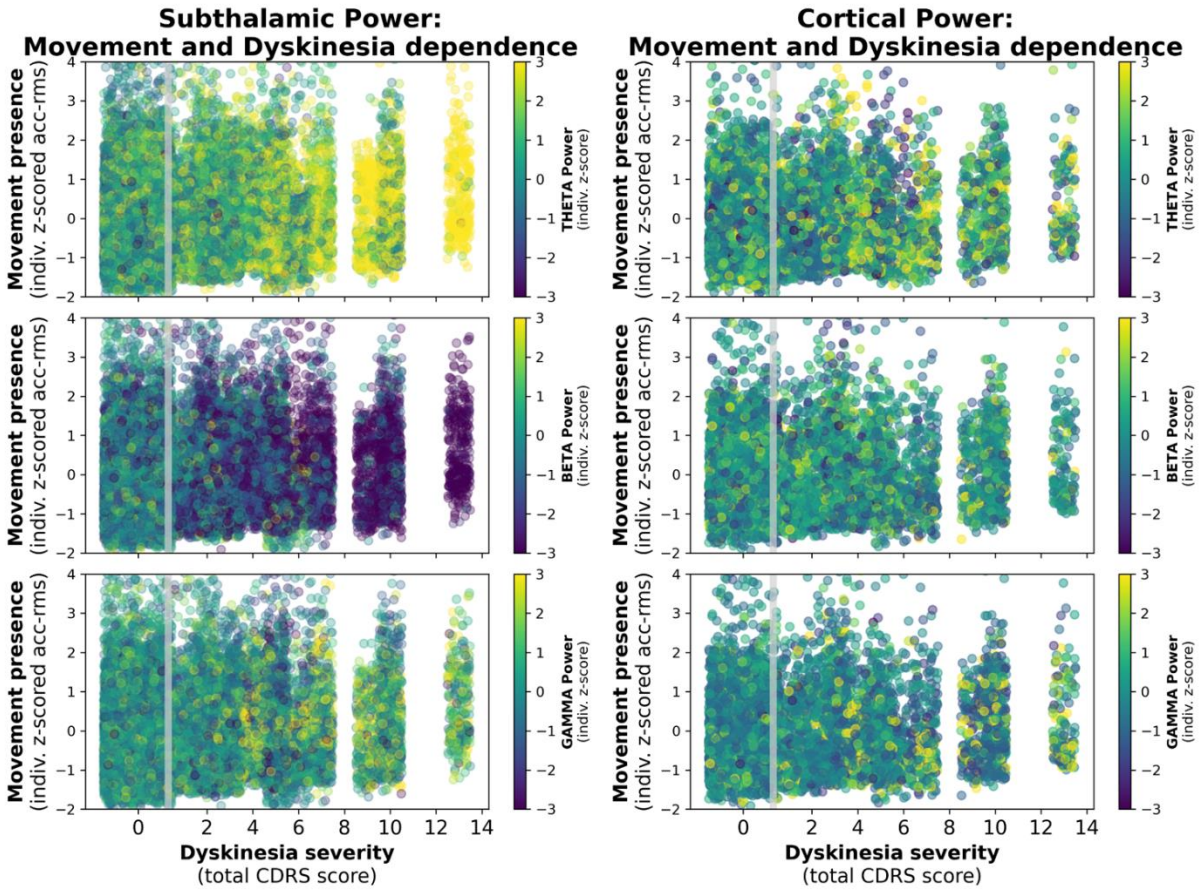

Figure 7: Cortical and subthalamic spectral powers and their linear dependencies on dyskinesia-severity and movement presence

The scatterplots demonstrate the modulation of theta (first row), low-beta (second row), and peak-gamma (third row) activity by dyskinesia severity (x-axis) and movement presence (y-axis). Subthalamic spectral activity is demonstrated in the left column, cortical spectral activity in the right column. Gamma activity seems to be more dependent on movement presence, whereas theta and beta modulations enhance with more severe dyskinesia. Local spectral power features were extracted from ten-second epochs of subthalamic data and averaged over bilateral STNs per epoch (left column) and cortical data (right column). Mean spectral powers are calculated per ten-second epoch (applying a 50%-overlap with consecutive ten-second epochs) and shown for the three main frequency bands of interest, i.e., theta band (4 – 8 Hz, first row), the low-beta range (12 – 20 Hz, second row), and the peak gamma range (5 Hz bin around an individual gamma-peak frequency, third row). Power values are individually z-scored and color-coded with yellow representing high values and blue representing low values. X-axes represent the absolute dyskinesia severity as total sum of the clinical dyskinesia rating scale (CDRS), including bilateral and axial dyskinetic manifestations. Y-axes represent the amount of movement present, as individually z-scored root mean squares from the bilateral accelerometer data.

Multivariate subthalamic features decode dyskinesia and movement influences predictions

Following the consistent modulation of subthalamic theta, beta, and gamma activity during dyskinetic periods (Figures 2, 4, and 7), we utilized each spectral band's direction of modulation to compose one single biomarker to decode dyskinesia periods:

$$\text{Oscillatory Dynamics Ratio} = \frac{\theta_{STN} * \gamma_{STN}}{\beta_{STN}}.$$

Formula 1: Composed multi-frequency biomarker to decode dyskinesia presence based on subthalamic theta-, beta-, and gamma-power.
The product of subthalamic theta power (4 – 8 Hz) and subthalamic peak-gamma power (individual gamma peak +/- 2.5 Hz) is divided by subthalamic low-beta power (12 – 20 Hz). All powers are calculated over ten-second epochs using Welch's method and are individually standardized over all recorded data. Bilateral subthalamic spectral power values were averaged per ten-second epoch and individually z-scored per frequency band over the full recording.

The Oscillatory Dynamics Ratio (ODR) biomarker (see Formula 1) leverages LID-associated subthalamic theta- and gamma-elevations and low-beta-attenuations and is expected to increase gradually during the rise of dopaminergic levels. To test the predictive potential of the ODR, all subthalamic recordings of subjects who experienced dyskinetic periods were included. All individual timelines were aligned to individual LID onset moments (Figure 8A). ODR values increased gradually after the intake of dopaminergic medication and showed a further increase after LID-onset compared to before LID onset. Then, ODR were calculated for all ten-second windows of all 21 subjects and a leave-one-subject-out cross validation was applied. For every iteration, an optimal linear ODR threshold for LID detection was determined in each training set (n=20) and tested on the remaining test subject. Using a linear regression, the ODR could predict LID presence with a mean balanced accuracy of 0.61 (sd: 0.14), with statistically significant predictions in eight out of twenty-one subjects.

The ODR (Formula 1 and Figure 8A) successfully differentiated between dyskinetic and non-dyskinetic periods in a sub population without requiring complex computational methods, which is advantageous for future clinical applications. However, it does not leverage the full spectrum of spectral features associated with LID observed before (Table 1, Figures 4 and 5). Therefore, we tested multivariate classifiers for LID detection with different combinations of spectral features. We compared classifiers based on subthalamic features, cortical features, and cortico-subthalamic features to identify the additional value of cortical data. For each feature set, both a linear logistic regression model (LM) and a non-linear convolutional neural network using a novel latency embedding method (CEBRA [48]) were applied (Fig S4). Since we recorded cortical data in only 13 out of 21 subjects, we first performed a head-to-head comparison of LID decoding based on only subthalamic (STN), only cortical (ECoG) and cortico-subthalamic (STN-ECoG) features in the 13 subjects with cortical recordings (Figure S4). All features were individually z-scored using the average and standard deviation from non-dyskinetic periods, in movement absence during the first 5 minutes after levodopa-intake. Both the subthalamic and cortico-subthalamic models, for both LM and CEBRA, outperformed the cortical models (Figures 8B and S4) (mean balanced accuracies: STN-LM: 0.76, sd: 0.12, STN-CEBRA: 0.77, sd: 0.14, STN-ECoG-LM: 0.75, sd: 0.12, and STN-ECoG-CEBRA: 0.72, sd: 0.15, ECOG-LM: 0.56, sd: 0.10, and ECOG-CEBRA: 0.58, sd: 0.11).
In a comparison between the ODR and the multivariate LM and CEBRA models, while maximizing our available data, the STN-CEBRA classifier detected LID presence with a significantly higher balanced accuracy than the STN-ODR (paired t-test stat: -3.87, p = 0.001) and the STN-LM (paired t-test stat: -4.18, p = 0.001) (Figures 7C and S4).

To better understand the predictive potential of the best performing classifier (STN-CEBRA), we investigated the influence of LID severity and the presence of movement on the LID detection. We categorized all subjects (n=21) based on their maximum LID severity observed, and compared the balanced accuracy distributions for different LID severities (Figure 8D). Although the relatively small number of included subjects per category limited statistical comparisons (two to six per category),

we did not see a difference in LID detection with respect to LID severity.
To assess the influence of movement presence on LID prediction, we sorted all ten-second windows based on the amount of activity captured by the accelerometers (i.e., individual z-scored accelerometer root mean squares, split in eight categories ranging from -2 to 4 sd). Within each movement activity range, we calculated individual positive and negative predictive values (respectively PPV and NPV). PPVs indicate what part of positive predictions (i.e. “LID is present”) is correct. NPVs indicate what part of negative predictions (i.e., “LID is not present”) is correct. Accordingly, the PPVs showed significantly more correct “LID present”-predictions with increasing movement presence (Spearman R = 0.27, p < 0.001), and NPVs showed a decreasing trend of the correctness with increasing movement presence (Spearman R = -0.07, p = 0.06) (Figure 8E).

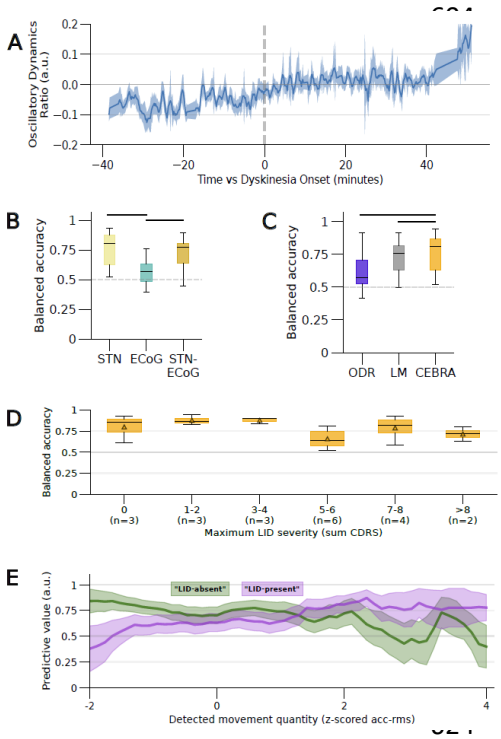

Figure 8: Performances of dyskinesia detection using different recording sites and models

The presence of LID was predicted using different classifier models combined with different combinations of data.
Panel A shows the temporal course of a single neural biomarker, composed of the product of subthalamic theta and gamma activity divided by subthalamic beta activity (Formula 1). Ratio values were calculated per second window. The time axis is individually corrected for LID onset. Subjects without LID are not included here. The shaded area represents the standard deviation.
Panel B shows the distributions of individual balanced accuracies for multivariate neural network-classifiers (CEBRA, see Methods) using only subthalamic data, only cortical data, or both. Only subjects with an ECoG electrode are included (n=13). Horizontal black lines between boxes indicate statistical difference in a paired t-test (alpha = 0.01, divided by 3 for multiple comparison correction.
Panel C shows the distributions of individual balanced accuracies for classifiers using the ratio biomarker (as shown in Panel A), a multivariate linear model (STN-LM), or a multivariate neural network (STN-CEBRA). Based on superiority of the STN data, only STN data for all subjects (n=21) are included.
Panel D shows the relation between the individual balanced accuracy of the LID prediction and the maximum LID severity observed within each subject. Only results of the STN CEBRA model are shown due to its superior performance. LID severity categories contain respectively 3, 3, 3, 6, 4, and 2 subjects. The horizontal black lines in the boxes represent the median and the colored triangles represent the mean of each box. The position on the x-axis categorizes the subjects on maximum LID severity as the maximum CDRS sum score assessed.
Panel E shows the distribution of positive and negative predictive values (respectively PPV and NPV) over different amounts of movement objectified in the accelerometer data. Only the STN CEBRA model is included based on its highest average performance. The x-axis is categorized based on z-scored individual accelerometer root mean squares and ranges from “No movement” (z-score -2 and less) to “Many movements” (z-score +4 and higher). The lines represent the distribution of individual PPV (green) and NPV (purple) values within the respective movement quantity. The NPV values show that the reliability, or the correctness, of “no LID present” predictions, shows a decreasing trend with increasing movement presence (Spearman R = -0.07, p = 0.06). Conversely, the PPV values show that the correctness of “LID present” predictions significantly increases with increasing movement presence (Spearman R = 0.27, p < 0.001).
a.u.: arbitrary units, bal. accuracy: balanced accuracy, CDRS: Clinical Dyskinesia Rating Scale, CEBRA: neural network using latent embedding (see Methods), ECoG: electrocorticography, LID: Levodopa-induced dyskinesia, LM: linear model, PPV: positive predictive value, STN: subthalamic nucleus, NPV: negative predicted value.

Discussion

We found a specific modulation of oscillatory theta, beta, and gamma band activity in STN and over motor cortical areas that was consistently associated with dyskinesia-provoking dopamine levels, and that showed specific modulation patterns in movement presence and absence during LID in PD patients. The respective oscillatory patterns could predict LID presence or absence, with STN activity being more accurate for LID prediction as compared to cortical neuronal patterns. Here, we propose an interpretation of our findings within a framework of systemic state changes [44]. A systemic state, of which there is only one at any given time for the entire system, integrates many other, more specific states, such as neural, behavioral, cardiac and others. These sub-states can vary in their spatial and temporal dynamics, which we can acknowledge by differentiating them into microstates (short-lasting) and macrostates (long-lasting). As such, all different sub-states form an integrated system responsible for specific behavior. Using neural deep brain recordings over an entire levodopa cycle that extends the dopaminergic dosage required for clinical benefit in our patients, we were able to measure neural and behavioral sub-states within periods of levodopa-induced dyskinesia (LID) for a defined time period by repeated measurements and as entire time-series. Our findings propose that dyskinetic periods can be interpreted as hyperdopaminergic macrostates that contain distinct microstates of movement presence and movement absence which can be objectified in cortico-subthalamic oscillatory activities. These microstates fit well to the clinically observed phenotype of LID.

Neural biomarkers have been identified in PD patients during dopaminergic modulation and LID [40,49–52], and are in line with the general pattern of oscillatory modulation of theta, beta and gamma band activity observed in our patients. Herein, increased theta and decreased beta band activity have been associated with periods of reduced motor inhibition, whereas gamma synchronization has been related to motor execution, in line with our concept of long-lasting macrostate changes and intermingled movement-specific microstate changes. Nevertheless, these temporal and behavioral aspects of neural biomarkers during LID with respect to involuntary movement periods have not been elucidated before. In order to interpret the specific behavioral relevance of the neuronal activity modulation observed during dyskinetic periods, we distinguished LID periods containing both movement presence and absence during the hyperdopaminergic state. We observed movement-independent bilateral theta increase and beta reduction of subthalamic neuronal activity that occur with the dopaminergic ON period but further increase during the dyskinetic period (Figure 4). Importantly, this slowly fluctuating macrostate change occurred bilaterally and was more prominent in periods without movements compared to movement presence suggesting that these changes are movement-independent and may rather balance motor inhibition and execution on a broader level.

Indeed, enhanced STN beta activity in PD has been characterized as a biomarker of bradykinesia and rigidity, i.e. serving as a 'anti-kinetic' rhythm within the cortical-STN network [53], that is reduced with levodopa treatment in parallel with motor improvement in PD [54,55]. During active behavioral motor inhibition [28], including reactive motor stopping in the non-dyskinetic state [43,56], beta activity has been described to increase [57–59], while beta desynchronization occurs during movement preparation, -execution and -imagery [28,55,60] suggesting that beta desynchronization is a prerequisite change in network activity for movements to occur [61]. In line with this concept, we observed a significant decrease in subthalamic beta activity during dyskinetic periods both during movement absence and movement presence (Figure 4), which fits previous reports of beta attenuation during LID in animals und patients [28,40,42,49–51]. Importantly, the beta activity attenuation in dyskinetic periods significantly extended the well-known beta attenuation during the medication ON state without LID (Figure 4) [31,55,62] and thus, is hypothesized to represent a hyperdopaminergic macrostate change of lowered motor inhibition that facilitates involuntary dyskinetic movements. This is further supported by the

692 significantly higher beta suppression with movement during LID as compared to movement during
693 non-dyskinetic periods and the significant decoupling of inter-STN beta activity. The robustness of
694 the LID-related beta attenuation regardless of movement presence, suggests that physiological and
695 dopamine-dependent movement-related low beta synchronization and desynchronization [43,63] may
696 adapt their magnitude during the hyperdopaminergic state. To further investigate the latter
697 however, the applied data-merging method (see Methods) limits the evaluation of single movement
698 effects. A described relation between LID severity and attenuations in cortical beta activity previously
699 observed in rodents [42], was not observed in our data. This may be explained by different recording
700 techniques, i.e. subdural ECoG recordings versus intracerebral recordings of cortical layers 5 and 6 in
701 the rodent study.
702

703 Theta activity has been found to increase with levodopa [64] and during dyskinesia in PD [37,40,50,51]. The
704 latter has been described as a constant activity change during biphasic as well as peak-dose
705 dyskinesia that was considered not movement-evoked [50,51]. In line with this, we found movement-
706 independent subthalamic theta activity increase during dyskinetic periods- underlining that the theta
707 increase is not associated with the abnormal movement itself. Strikingly, the subthalamic theta
708 increase in dyskinetic periods was more pronounced during movement absence. Additionally, our
709 data show that STN theta increase correlated with LID severity (Figure 4 and 7). This is similar to
710 observations in other hyperkinetic disorders such as dystonia, where theta activity is an established
711 biomarker [65] with pallidal activity driving EMG in dystonic muscles [66] and increased theta power and
712 coherence within the striato-pallidal loop correlates with severity of dystonic symptoms [67]. On the
713 cortical level, this relationship has so far only been described using EEG data in a few patients [50], but
714 a recent ECoG study did not show improved dyskinesia prediction incorporating cortical theta activity
715 in the model [40]. Similar to the latter, we did not find theta modulation with dyskinesia on the cortical
716 level, but cortico-STN coherence increased in the theta band during dyskinetic periods in our patients
717 supporting an involvement of the cortico-STN network in this frequency band. This would also be in
718 line with functional MRI data reporting reduction in dyskinesia during inhibitory pre-SMA repetitive
719 transcranial stimulation, an area that was hyperactive after levodopa intake in PD prior to occurrence
720 of dyskinesia [45,68].

721 Nevertheless, subthalamic theta elevation and increased cortico-STN theta coherence has also been
722 described during task-related successful active movement suppression in PD [43] and successful
723 suppression of involuntary tics were associated with increased cortical theta band coherence [69].
724 Furthermore, elevations of subthalamic theta and inferior frontal cortex EEG power are reported
725 during cognitive states of decision making during conflict [37,38,70], where STN activity has been
726 associated with active suppression of premature responses [71,72]. Accordingly, stimulation of the STN
727 can increase the number of incorrect responses under conflict [73] or premature responses in motor
728 inhibition tasks [74,75]. These findings support an association of subthalamic theta activity with motor
729 and non-motor inhibition including motor intention or involuntary movements. The functional role of
730 theta activity seems more complex and its topographical distribution in STN recordings is more
731 variable including non-motor ventral contacts during cognitive processing but also dyskinesia [37,50].
732 Whether task-related theta modulation more prominent in the motor-cognitive domain has a
733 different functional role as compared to theta activity recorded within the motor cortical-basal
734 ganglia loop during hyperkinesia cannot be answered with the current data available. Our analysis
735 suggests that an increase in theta oscillatory activity can serve as a biomarker for the slow
736 macrostate shift towards the dyskinetic state independent of movement presence per se.

737 Within this macrostate of lowered motor inhibition, single dyskinetic movements occur (Figure 1)
738 that showed an association with the increase in local subthalamic and cortical gamma activity and

739 cortico-subthalamic gamma coherence in our patients (Figure 4 and 5). Narrowband gamma
740 synchronization is the most established LID-related biomarker in both subthalamic [37,40,42,49,50] and
741 cortical [39–41,76] recordings and is considered a 'pro-kinetic' activity [53]. Importantly, we show for the
742 first time a distinct movement-dependence of gamma activity associated with LID as we
743 differentiated between movement presence and movement absence in dyskinetic periods. Previous
744 findings on gamma synchronization during LID lack this information as current dyskinetic animal
745 models typically lack movement absence recordings during dyskinetic periods [77], similar to recent
746 naturalistic patient recordings without continuous movement monitoring on a second-scale
747 resolution [40]. Within our framework of macro- and microstate integrated state dynamics, we
748 interpret these movements during dyskinetic periods as fast-changing microstates integrated in the
749 complex phenotype of LID, which are represented by gamma elevations in bilateral STNs and the
750 cortex contralateral to dyskinetic body sides. Movement execution has been closely associated with
751 gamma synchronization on basal ganglia and cortical level suggesting that gamma increase may scale
752 with the speed or vigor of voluntary movements [35,36,60,78–81]. During a hyperdopaminergic state of
753 reduced motor inhibition an imbalance of reduced beta activity and excessive prokinetic gamma
754 synchronization may lead to dyskinesia. Nevertheless, it is not yet clear if narrowband gamma
755 oscillations cause dyskinesia or are simply a physiological short-lived correlate of (excessive)
756 movements. In our patients, the strictly contralateral cortical gamma synchronization scaled with the
757 dyskinesia severity and further supports that it can be used as a fast-tracking biomarker for
758 movement activity [40]. However, its contralateral expression opposed to dyskinetic movement makes
759 it less robust as a biomarker in daily life and would suggest bilateral cortical recording hardware.

760 Subthalamic gamma activity has been argued to not merely effect movement execution, but also
761 motor stopping [82]. Since the clinical phenotype of LID includes active motor stopping as patients'
762 typically intent to terminate involuntary movements, the observed decrease in cortical gamma
763 activity during movement absence in the dyskinetic state may also be explained in parallel to
764 reported decreases in subthalamic and thalamic gamma activity during successful intentional motor
765 inhibition [43,83].

766 Together, fast changing movement-dependent gamma-magnitudes could be modulated by
767 underlying slower bilateral theta and beta rhythm fluctuations,[84] which would comply with the here
768 suggested framework of interpreting the complex motor network activity associated with LID into
769 macro- and microstate changes. The movement-independence of the bilateral subthalamic theta and
770 beta patterns supports our hypothesis that they represent a slow fluctuating macrostate of lowered
771 motor inhibition that leads to an increased likelihood of movement to occur. The movement
772 dependence of the STN and cortical gamma patterns suggest a more volatile and fast-changing
773 pathophysiological role that is more lateralized within the cortico-STN network and on the cortical
774 level. Thus, we suggest dyskinetic movements to occur as fast-changing microstates represented by
775 gamma activity changes, parallel to a slow-changing hyperdopaminergic macrostate of lowered
776 motor inhibition represented by a reduction in beta and increase in theta activity within the cortico-
777 STN network.

778 The hypothesized macro- and microstates fit into current fundamental principles and frameworks of
779 motor inhibition within the cortico-basal-ganglia motor network. The striatal motor network lowers
780 its motor inhibition under chronic dopaminergic depletion by adapting the SPN-architecture [17] and
781 the GABAergic [18,20] and glutamatergic [19,85] striatal projections. The hypothesized relevance of these
782 striatal changes for the pathophysiology of LID [86,87], was recently confirmed by studies showing that
783 imbalanced clusters of direct- and indirect-SPN and structural hypertrophy of SPNs allow the
784 occurrence of LID [22,25]. More specifically, parvalbumin-expressing (PV+) FSIs have been attributed
785 importance in motor control [88,89], striatal neuronal ensembles reconfiguration [90], and gamma

786 oscillation plasticity [91]. A recently discovered PV+ selective subthalamo-striatal projection [92] and the
787 presence of PV+ glutamatergic interneurons specifically in the dorsolateral STN [93,94], may underline
788 the importance of PV+ FSIs in STN DBS' sweet spot for pro-kinetic effects [9].
789 The abovementioned studies provide fundamental evidence on compensatory motor disinhibition in
790 PD and its association with LID occurrence. Moreover, the FSI-changes may explain the characteristic
791 gamma activity during dyskinetic movement.

792 Since LID is a common target for adaptive DBS [95], the demonstrated clinical relevance of
793 neurophysiological biomarkers can inform future adaptive DBS (aDBS) strategies, especially to
794 improve spatial and temporal characteristics of different closed-loop feedback mechanisms such as
795 fast versus slow aDBS [96]. The demonstrated differences between cortical and basal ganglia spectral
796 patterns during LID suggest that cortical biomarkers are sensible for fast aDBS algorithms that react
797 to microstate changes, but may lose the specificity and effect with slow adapting algorithms. For the
798 latter, subthalamic biomarkers may suit better using beta and theta band as biomarkers of
799 macrostate changes. For example, in case a fast aDBS algorithm is targeted at movement-dependent
800 cortical gamma activity, the volatile, non-continuous nature of movements has to be incorporated in
801 the aDBS decision making process. The superiority of our subthalamic multivariate prediction model
802 over the single ratio-biomarker and the cortical multivariate models (Figure 8BC), suggests that slow
803 aDBS models (i.e., ten-second windows) do not profit from additional cortical features and perform
804 best using computational heavier multivariate classifiers. The superiority of subthalamic features
805 over cortical features to detect LID presence we hypothesize to be a result of the ten-second window
806 length that favors slow network activity changes. We could therefore hypothesize that the
807 prerequisite for dyskinesia to occur depends on the slower neural activity change at the level of the
808 basal ganglia, which is in line with described discharge pattern changes within the striato-pallidal
809 loop [22]. Microstate changes will not be preferentially detected in our prediction model due to the
810 selected relatively long window length that inevitably leads to the merging of microstates of
811 movement presence with periods of movement absence within the same window for prediction.
812 Cortical features are therefore expected to have more predictive value in fast-aDBS strategies,
813 applying shorter window lengths, and thus isolating separate microstates of movement presence.
814 The latter is supported by earlier work showing that cortical features had more predictive value than
815 subthalamic features in movement prediction on a sub-second temporal scale [35,97].
816 Additionally we could demonstrate that the amount of movement presence within a ten-second
817 window significantly affected the predictive performance of LID detection, since positive LID-present
818 predictions were significantly more reliable in windows containing more movement (Figure 8E).
819 These findings underline the distinct character of the behavioral states of movement presence and
820 absence within a dyskinetic state and suggest that future daily life LID detection models will benefit
821 from a separate movement classifier.
822 The demonstrated level of neurophysiological and behavioral detail was the result of invasive cortico-
823 subthalamic recordings in PD patients in an in-clinic controlled environment. We addressed several
824 analytical challenges resulting from heterogeneous individual pharmacodynamics during a LID-
825 provoking protocol in PD patients. The before mentioned methodological challenges in rodent and
826 naturalistic, resp. a lack of movement absence during LID [21,77] or a lack of dyskinetic movement
827 monitoring [98], underlines the importance of this translational human research to bridge the gap to
828 valid real-world applications. Multimodal naturalistic monitoring methods such as wearables sensors
829 and ecological valid patient reported outcomes can be applied as naturalistic proxies for kinematic
830 and clinical observations [99–101].

831 Our findings propose a conceptual adaptation of the interpretation of neurophysiological biomarkers
832 for LID. Distinct spatial, temporal, and spectral neural patterns are associated with distinct clinically

relevant behavioral states. A slow movement-independent macrostate change is hypothesized to occur with levodopa that is represented by bilateral modulation in theta and beta subthalamic patterns, whereas a volatile, movement-dependent microstate is associated with fast-adapting modulation in cortico-subthalamic gamma activity occurring with the dyskinetic movement itself. The observed movement-independent spatial and spectral findings characterizing the dyskinetic state fit well into current pathophysiological concepts of an overcompensated motor disinhibition in PD that can allow for LID to occur. Finally, this improved behavioral understanding of these biomarkers aims to tailor future aDBS to their specific clinical purposes to optimally serve PD patients during real-life.

Acknowledgements

We would like to thank the patients that participated in the study. We would like to thank Ulrike Uhlig for her help with organizing and assisting during the recordings. A.A.K. received funding from the Lundbeck Foundation as part of the collaborative project grant “Adaptive and precise targeting of cortex-basal ganglia circuits in Parkinson´s Disease” (Grant Nr. R336-2020-1035), from the Forschungsgemeinschaft (D.F.G., German Research Foundation) – Project-ID 424778381 – TRR 295, and from the Deutsche Forschungsgemeinschaft (DFG, German Research Foundation) under Germany´s Excellence Strategy – EXC-2049 – 390688087. P.T. received funding from the D.F.G. in Project-IDs: 433490190, 426503586, 424778381, and 426503586. WJN received funding from the European Union (ERC, ReinforceBG, project 101077060), DFG – Project-ID 424778381 – TRR 295 and the Bundesministerium für Bildung und Forschung (BMBF, project FKZ01GQ1802). J.H., R.L., and J.L.B. are fellows of BIH Charité Clinician Scientist Programs. J.H. is a postdoctoral fellow of the Parkinson Foundation.

Author contributions

J.H., R.L., and A.A.K. conceptualized and designed the study. J.H., R.L., V.M., R.K., J.B. performed the electrophysiological recordings. K.F. and G.S. performed the neurosurgical procedures. P.K. assessed all clinical dyskinesia scores. J.H. conducted the electrophysiological, movement, and statistical analysis and drafted the study. T.B. assisted in the coherence analyses. J.H. and T.M. performed the machine learning analyses, A.A.K. and J.N. supervised these analyses. J.H., P.T., and A.A.K., contributed to the interpretation of the data, revised, and edited the work critically. J.H., V.M., and A.M. created the visualizations and performed clinical data acquisition. A.A.K. contributed critically to the supervision, project organization and funding acquisition. All coauthors have reviewed and approved the content of the manuscript.

Financial disclosures

A.A.K. received honoraria for consultancies and/or talks from Medtronic, Boston Scientific, and Stada Pharm. PK received speaker´s honoraria from Medtronic and Stadapharm and is in the Advisory Board of Abbott and Stadapharm, outside the submitted work. WJN received honoraria for consulting from InBrain – Neuroelectronics that is a neurotechnology company and honoraria for talks from Medtronic that is a manufacturer of deep brain stimulation devices unrelated to this manuscript. JB received financial compensation for serving on an advisory board from Medtronic.

875 **References**

876 1. Voon, V. *et al.* Impulse control disorders and levodopa-induced dyskinesias in Parkinson's disease: an
877 update. *Lancet Neurol.* **16**, 238–250 (2017).
878 2. Jankovic, J. Motor fluctuations and dyskinesias in Parkinson's disease: clinical manifestations. *Mov Disord*
879 **20 Suppl 11**, S11-6 (2005).
880 3. Hechtner, M. C. *et al.* Quality of life in Parkinson's disease patients with motor fluctuations and dyskinesias
881 in five European countries. *Parkinsonism Relat. Disord.* **20**, 969–974 (2014).
882 4. de Bie, R. M. A., Clarke, C. E., Espay, A. J., Fox, S. H. & Lang, A. E. Initiation of pharmacological therapy in
883 Parkinson's disease: when, why, and how. *Lancet Neurol.* **19**, 452–461 (2020).
884 5. di Biase, L., Pecoraro, P. M., Carbone, S. P., Caminiti, M. L. & Di Lazzaro, V. Levodopa-Induced Dyskinesias
885 in Parkinson's Disease: An Overview on Pathophysiology, Clinical Manifestations, Therapy Management
886 Strategies and Future Directions. *J. Clin. Med.* **12**, 4427 (2023).
887 6. Espa, E., Song, L., Skovgård, K., Fanni, S. & Cenci, M. A. Dopamine Agonist Cotreatment Alters
888 Neuroplasticity and Pharmacology of Levodopa-Induced Dyskinesia. *Mov. Disord.* **38**, 410–422 (2023).
889 7. Lachenmayer, M. L. *et al.* Subthalamic and pallidal deep brain stimulation for Parkinson's disease-meta-
890 analysis of outcomes. *NPJ Park. Dis.* **7**, 77 (2021).
891 8. Kübler, D. *et al.* Gender-specific outcomes of deep brain stimulation for Parkinson's disease — results from
892 a single movement disorder center. *Neurol. Sci.* **44**, 1625–1631 (2023).
893 9. Tödt, I. *et al.* The Contribution of Subthalamic Nucleus Deep Brain Stimulation to the Improvement in
894 Motor Functions and Quality of Life. *Mov. Disord. Off. J. Mov. Disord. Soc.* **37**, 291–301 (2022).
895 10. Pürner, D. *et al.* Nationwide Retrospective Analysis of Combinations of Advanced Therapies in Patients
896 With Parkinson Disease. *Neurology* **101**, e2078–e2093 (2023).
897 11. Sriram, A. *et al.* Brittle Dyskinesia Following STN but not GPi Deep Brain Stimulation. **4**, 242 (2014).
898 12. Mainardi, M. *et al.* Deep brain stimulation of globus pallidus internus and subthalamic nucleus in
899 Parkinson's disease: a multicenter, retrospective study of efficacy and safety. *Neurol. Sci. Off. J. Ital.*
900 *Neurol. Soc. Ital. Soc. Clin. Neurophysiol.* **45**, 177–185 (2024).
901 13. Weiss, D. *et al.* Changing Gears - DBS For Dopaminergic Desensitization in Parkinson's Disease? *Ann.*
902 *Neurol.* **90**, 699–710 (2021).
903 14. Picconi, B. *et al.* Loss of bidirectional striatal synaptic plasticity in L-DOPA–induced dyskinesia. *Nat.*
904 *Neurosci.* **6**, 501–506 (2003).
905 15. Bove, F. *et al.* Neuroplasticity in levodopa-induced dyskinesias: An overview on pathophysiology and
906 therapeutic targets. *Prog. Neurobiol.* **232**, 102548 (2024).
907 16. Cenci, M. A. & Kumar, A. Cells, pathways, and models in dyskinesia research. *Curr. Opin. Neurobiol.* **84**,
908 102833 (2024).
909 17. Gomez, G. *et al.* Changes in Dendritic Spine Density and Inhibitory Perisomatic Connectivity onto Medium
910 Spiny Neurons in L-Dopa-Induced Dyskinesia. *Mol. Neurobiol.* **56**, 6261–6275 (2019).
911 18. Fino, E., Vandecasteele, M., Perez, S., Saudou, F. & Venance, L. Region-specific and state-dependent action
912 of striatal GABAergic interneurons. *Nat. Commun.* **9**, 3339 (2018).
913 19. Campanelli, F., Natale, G., Marino, G., Ghiglieri, V. & Calabresi, P. Striatal glutamatergic hyperactivity in
914 Parkinson's disease. *Neurobiol. Dis.* **168**, 105697 (2022).
915 20. Mallet, N., Ballion, B., Moine, C. L. & Gonon, F. Cortical Inputs and GABA Interneurons Imbalance
916 Projection Neurons in the Striatum of Parkinsonian Rats. *J. Neurosci.* **26**, 3875–3884 (2006).
917 21. Alcacer, C. *et al.* Abnormal hyperactivity of specific striatal ensembles encodes distinct dyskinetic
918 behaviors revealed by high-resolution clustering. 2024.09.06.611664 Preprint at
919 https://doi.org/10.1101/2024.09.06.611664 (2024).
920 22. Parker, J. G. *et al.* Diametric neural ensemble dynamics in parkinsonian and dyskinetic states. *Nature* **557**,
921 177–182 (2018).
922 23. Thiele, S. L. *et al.* Selective loss of bi-directional synaptic plasticity in the direct and indirect striatal output
923 pathways accompanies generation of parkinsonism and l-DOPA induced dyskinesia in mouse models.
924 *Neurobiol. Dis.* **71**, 334–344 (2014).
925 24. Alcacer, C. *et al.* Chemogenetic stimulation of striatal projection neurons modulates responses to
926 Parkinson's disease therapy. *J. Clin. Invest.* **127**, 720–734 (2017).
927 25. Abe, Y. *et al.* Shared GABA transmission pathology in dopamine agonist- and antagonist-induced
928 dyskinesia. *Cell Rep. Med.* **4**, 101208 (2023).
929 26. Ryan, M. B. *et al.* Excessive firing of dyskinesia-associated striatal direct pathway neurons is gated by
930 dopamine and excitatory synaptic input. *Cell Rep.* **43**, (2024).

27. Polyakova, Z., Hatanaka, N., Chiken, S. & Nambu, A. Subthalamic Activity for Motor Execution and Cancelation in Monkeys. *J. Neurosci. Off. J. Soc. Neurosci.* **44**, e1911222024 (2024).
28. Kühn, A. A. *et al.* Event-related beta desynchronization in human subthalamic nucleus correlates with motor performance. *Brain J. Neurol.* **127**, 735–746 (2004).
29. Callahan, J. W. *et al.* Movement-related increases in subthalamic activity optimize locomotion. *Cell Rep.* **43**, 114495 (2024).
30. Lofredi, R. *et al.* Subthalamic stimulation impairs stopping of ongoing movements. *Brain J. Neurol.* **144**, 44–52 (2021).
31. Neumann, W.-J., Gilron, R., Little, S. & Tinkhauser, G. Adaptive Deep Brain Stimulation: From Experimental Evidence Toward Practical Implementation. *Mov. Disord.* **38**, 937–948 (2023).
32. Kühn, A. A., Kupsch, A., Schneider, G.-H. & Brown, P. Reduction in subthalamic 8-35 Hz oscillatory activity correlates with clinical improvement in Parkinson's disease. *Eur. J. Neurosci.* **23**, 1956–1960 (2006).
33. Lofredi, R. *et al.* Pallidal Beta Activity Is Linked to Stimulation-Induced Slowness in Dystonia. *Mov. Disord. Off. J. Mov. Disord. Soc.* **38**, 894–899 (2023).
34. Herz, D. M. *et al.* Dynamic control of decision and movement speed in the human basal ganglia. *Nat. Commun.* **13**, 7530 (2022).
35. Merk, T. *et al.* Electrocorticography is superior to subthalamic local field potentials for movement decoding in Parkinson's disease. *eLife* **11**, e75126 (2022).
36. Lofredi, R. *et al.* Dopamine-dependent scaling of subthalamic gamma bursts with movement velocity in patients with Parkinson's disease. *eLife* **7**, e31895 (2018).
37. Rodriguez-Oroz, M. C. *et al.* Involvement of the subthalamic nucleus in impulse control disorders associated with Parkinson's disease. *Brain* **134**, 36–49 (2011).
38. Zavala, B. A. *et al.* Midline frontal cortex low-frequency activity drives subthalamic nucleus oscillations during conflict. *J. Neurosci. Off. J. Soc. Neurosci.* **34**, 7322–7333 (2014).
39. Halje, P. *et al.* Levodopa-Induced Dyskinesia Is Strongly Associated with Resonant Cortical Oscillations. *J. Neurosci.* **32**, 16541–16551 (2012).
40. Olaru, M. *et al.* Motor network gamma oscillations in chronic home recordings predict dyskinesia in Parkinson's disease. *Brain* awae004 (2024) doi:10.1093/brain/awae004.
41. Swann, N. C. *et al.* Gamma Oscillations in the Hyperkinetic State Detected with Chronic Human Brain Recordings in Parkinson's Disease. *J Neurosci* **36**, 6445–58 (2016).
42. Dupre, K. B. *et al.* Effects of L-dopa priming on cortical high beta and high gamma oscillatory activity in a rodent model of Parkinson's disease. *Neurobiol. Dis.* **86**, 1–15 (2016).
43. Alegre, M. *et al.* The subthalamic nucleus is involved in successful inhibition in the stop-signal task: a local field potential study in Parkinson's disease. *Exp. Neurol.* **239**, 1–12 (2013).
44. Signoret-Genest, J. *et al.* Integrated cardio-behavioral responses to threat define defensive states. *Nat. Neurosci.* **26**, 447–457 (2023).
45. Herz, D. M. *et al.* The acute brain response to levodopa heralds dyskinesias in Parkinson disease. *Ann. Neurol.* **75**, 829–836 (2014).
46. Hagell, P. & Widner, H. Clinical rating of dyskinesias in Parkinson's disease: use and reliability of a new rating scale. *Mov. Disord. Off. J. Mov. Disord. Soc.* **14**, 448–455 (1999).
47. Nikulin, V. V., Nolte, G. & Curio, G. A novel method for reliable and fast extraction of neuronal EEG/MEG oscillations on the basis of spatio-spectral decomposition. *NeuroImage* **55**, 1528–1535 (2011).
48. Schneider, S., Lee, J. H. & Mathis, M. W. Learnable latent embeddings for joint behavioural and neural analysis. *Nature* **617**, 360–368 (2023).
49. Fogelson, N. *et al.* Reciprocal interactions between oscillatory activities of different frequencies in the subthalamic region of patients with Parkinson's disease. *Eur. J. Neurosci.* **22**, 257–266 (2005).
50. Alonso-Frech, F. *et al.* Slow oscillatory activity and levodopa-induced dyskinesias in Parkinson's disease. *Brain* **129**, 1748–1757 (2006).
51. Alegre, M. *et al.* Subthalamic activity during diphasic dyskinesias in Parkinson's disease. *Mov. Disord.* **27**, 1178–1181 (2012).
52. Gilron, R. *et al.* Long-term wireless streaming of neural recordings for circuit discovery and adaptive stimulation in individuals with Parkinson's disease. *Nat. Biotechnol.* (2021) doi:10.1038/s41587-021-00897-5.
53. Brown, P. *et al.* Dopamine Dependency of Oscillations between Subthalamic Nucleus and Pallidum in Parkinson's Disease. *J. Neurosci.* **21**, 1033–1038 (2001).
54. Lofredi, R. *et al.* Subthalamic beta bursts correlate with dopamine-dependent motor symptoms in 106 Parkinson's patients. *Npj Park. Dis.* **9**, 1–9 (2023).

55. Kuhn, A. A., Kupsch, A., Schneider, G. H. & Brown, P. Reduction in subthalamic 8-35 Hz oscillatory activity correlates with clinical improvement in Parkinson's disease. *Eur J Neurosci* **23**, 1956–60 (2006).
56. Horst, J. ter, Boillot, M., Cohen, M. X. & Englitz, B. Decreased Beta Power and OFC–STN Phase Synchronization during Reactive Stopping in Freely Behaving Rats. *J. Neurosci.* **44**, (2024).
57. Cao, C. *et al.* Low-beta versus high-beta band cortico-subcortical coherence in movement inhibition and expectation. *Neurobiol. Dis.* **201**, 106689 (2024).
58. Wessel, J. R. *et al.* Stop-related subthalamic beta activity indexes global motor suppression in Parkinson's disease. *Mov. Disord.* **31**, 1846–1853 (2016).
59. Aron, A. R., Herz, D. M., Brown, P., Forstmann, B. U. & Zaghloul, K. Frontosubthalamic Circuits for Control of Action and Cognition. *J. Neurosci.* **36**, 11489–11495 (2016).
60. Androulidakis, A. G. *et al.* Dopaminergic therapy promotes lateralized motor activity in the subthalamic area in Parkinson's disease. *Brain J. Neurol.* **130**, 457–468 (2007).
61. Williams, D. *et al.* Dopamine-dependent changes in the functional connectivity between basal ganglia and cerebral cortex in humans. *Brain* **125**, 1558–1569 (2002).
62. Kuhn, A. A. *et al.* High-frequency stimulation of the subthalamic nucleus suppresses oscillatory beta activity in patients with Parkinson's disease in parallel with improvement in motor performance. *J Neurosci* **28**, 6165–73 (2008).
63. Mathiopoulou, V. *et al.* Modulation of subthalamic beta oscillations by movement, dopamine, and deep brain stimulation in Parkinson's disease. *Npj Park. Dis.* **10**, 1–7 (2024).
64. Priori, A. *et al.* Rhythm-specific pharmacological modulation of subthalamic activity in Parkinson's disease. *Exp Neurol* **189**, 369–79 (2004).
65. Neumann, W.-J. *et al.* A localized pallidal physiomarker in cervical dystonia. *Ann. Neurol.* **82**, 912–924 (2017).
66. Sharott, A. *et al.* Is the synchronization between pallidal and muscle activity in primary dystonia due to peripheral afferance or a motor drive? *Brain J. Neurol.* **131**, 473–484 (2008).
67. Lofredi, R. *et al.* Striato-pallidal oscillatory connectivity correlates with symptom severity in dystonia patients. *Nat. Commun.* **15**, 8475 (2024).
68. Lohse, A. *et al.* Low-frequency transcranial stimulation of pre-supplementary motor area alleviates levodopa-induced dyskinesia in Parkinson's disease: a randomized cross-over trial. *Brain Commun.* **2**, fcaa147 (2020).
69. Serrien, D. J., Orth, M., Evans, A. H., Lees, A. J. & Brown, P. Motor inhibition in patients with Gilles de la Tourette syndrome: functional activation patterns as revealed by EEG coherence. *Brain* **128**, 116–125 (2005).
70. Cavanagh, J. F. *et al.* Subthalamic nucleus stimulation reverses mediofrontal influence over decision threshold. *Nat. Neurosci.* **14**, 1462–1467 (2011).
71. Frank, M. J., Samanta, J., Moustafa, A. A. & Sherman, S. J. Hold Your Horses: Impulsivity, Deep Brain Stimulation, and Medication in Parkinsonism. *Science* **318**, 1309–1312 (2007).
72. Herz, D. M., Frank, M. J., Tan, H. & Groppa, S. Subthalamic control of impulsive actions: insights from deep brain stimulation in Parkinson's disease. *Brain* **147**, 3651–3664 (2024).
73. Green, N. *et al.* Reduction of Influence of Task Difficulty on Perceptual Decision Making by STN Deep Brain Stimulation. *Curr. Biol.* **23**, 1681–1684 (2013).
74. Ballanger, B. *et al.* Release your horses: Deep Brain Stimulation of the subthalamic nucleus improves motor functions at the expense of response inhibition. A H215O PET study. *NeuroImage* **47**, S115 (2009).
75. Wylie, S. A. *et al.* Subthalamic nucleus stimulation influences expression and suppression of impulsive behaviour in Parkinson's disease. *Brain* **133**, 3611–3624 (2010).
76. Güttler, C. *et al.* Levodopa-Induced Dyskinesia Are Mediated by Cortical Gamma Oscillations in Experimental Parkinsonism. *Mov. Disord. Off. J. Mov. Disord. Soc.* **36**, 927–937 (2021).
77. Ye, T., Bartlett, M. J., Sherman, S. J., Falk, T. & Cowen, S. L. Spectral signatures of L-DOPA-induced dyskinesia depend on L-DOPA dose and are suppressed by ketamine. *Exp. Neurol.* **340**, 113670 (2021).
78. Alegre, M. *et al.* Movement-related changes in oscillatory activity in the human subthalamic nucleus: ipsilateral vs. contralateral movements. *Eur. J. Neurosci.* **22**, 2315–2324 (2005).
79. Brücke, C. *et al.* Scaling of movement is related to pallidal γ oscillations in patients with dystonia. *J. Neurosci. Off. J. Soc. Neurosci.* **32**, 1008–1019 (2012).
80. Crone, N. E. *et al.* Functional mapping of human sensorimotor cortex with electrocorticographic spectral analysis. I. Alpha and beta event-related desynchronization. *Brain J. Neurol.* **121 (Pt 12)**, 2271–2299 (1998).
81. Cassidy, M. *et al.* Movement-related changes in synchronization in the human basal ganglia. *Brain* **125**, 1235–1246 (2002).

82. Fischer, P. *et al.* Subthalamic nucleus gamma activity increases not only during movement but also during movement inhibition. *eLife* **6**, e23947 (2017).
83. Brücke, C. *et al.* Thalamic gamma oscillations correlate with reaction time in a Go/noGo task in patients with essential tremor. *NeuroImage* **75**, 36–45 (2013).
84. Buzsáki, G. & Wang, X.-J. Mechanisms of gamma oscillations. *Annu. Rev. Neurosci.* **35**, 203–225 (2012).
85. Hutchison, M. A. *et al.* Genetic inhibition of neurotransmission reveals role of glutamatergic input to dopamine neurons in high-effort behavior. *Mol. Psychiatry* **23**, 1213–1225 (2018).
86. Gittis, A. H., Nelson, A. B., Thwin, M. T., Palop, J. J. & Kreitzer, A. C. Distinct Roles of GABAergic Interneurons in the Regulation of Striatal Output Pathways. *J. Neurosci.* **30**, 2223–2234 (2010).
87. Gittis, A. H. *et al.* Selective Inhibition of Striatal Fast-Spiking Interneurons Causes Dyskinesias. *J. Neurosci.* **31**, 15727–15731 (2011).
88. Koós, T. & Tepper, J. M. Inhibitory control of neostriatal projection neurons by GABAergic interneurons. *Nat. Neurosci.* **2**, 467–472 (1999).
89. Jung, K. *et al.* An adaptive behavioral control motif mediated by cortical axo-axonic inhibition. *Nat. Neurosci.* **26**, 1379–1393 (2023).
90. Duhne, M. *et al.* Activation of parvalbumin-expressing neurons reconfigures neuronal ensembles in murine striatal microcircuits. *Eur. J. Neurosci.* **53**, 2149–2164 (2021).
91. Hadler, M. D., Tzilivaki, A., Schmitz, D., Alle, H. & Geiger, J. R. P. Gamma oscillation plasticity is mediated via parvalbumin interneurons. *Sci. Adv.* **10**, eadj7427 (2024).
92. Kondabolu, K. *et al.* A Selective Projection from the Subthalamic Nucleus to Parvalbumin-Expressing Interneurons of the Striatum. *eNeuro* **10**, ENEURO.0417-21.2023 (2023).
93. Jeon, H. *et al.* Topographic connectivity and cellular profiling reveal detailed input pathways and functionally distinct cell types in the subthalamic nucleus. *Cell Rep.* **38**, 110439 (2022).
94. Lévesque, J.-C. & Parent, A. GABAergic interneurons in human subthalamic nucleus. *Mov. Disord. Off. J. Mov. Disord. Soc.* **20**, 574–584 (2005).
95. Oehrn, C. R. *et al.* Chronic adaptive deep brain stimulation versus conventional stimulation in Parkinson's disease: a blinded randomized feasibility trial. *Nat. Med.* 1–12 (2024) doi:10.1038/s41591-024-03196-z.
96. Little, S. & Brown, P. Debugging Adaptive Deep Brain Stimulation for Parkinson's Disease. *Mov. Disord. Off. J. Mov. Disord. Soc.* **35**, 555–561 (2020).
97. Köhler, R. M. *et al.* Dopamine and deep brain stimulation accelerate the neural dynamics of volitional action in Parkinson's disease. *Brain J. Neurol.* awae219 (2024) doi:10.1093/brain/awae219.
98. Ancona, S. *et al.* Wearables in the home-based assessment of abnormal movements in Parkinson's disease: a systematic review of the literature. *J. Neurol.* **269**, 100–110 (2022).
99. Heijmans, M. *et al.* Monitoring Parkinson's disease symptoms during daily life: a feasibility study. *NPJ Park. Dis* **5**, 21 (2019).
100. Feldmann, L. K., Roudini, J., Kühn, A. A. & Habets, J. G. V. Improving naturalistic neuroscience with patient engagement strategies. *Front. Hum. Neurosci.* **17**, (2024).
101. Kamo, H. *et al.* A proof of concept: digital diary using 24-hour monitoring using wearable device for patients with Parkinson's disease in nursing homes. *Front. Neurol.* **15**, 1356042 (2024).

1087 **Methods**

1088 *Patient inclusions and characteristics*

1089 We recruited 21 patients that underwent implantation of bilateral STN DBS electrodes as a treatment
1090 for idiopathic Parkinson's disease at the Movement Disorders and Neuromodulation Unit of the
1091 Charité University Medicine Hospital. We excluded patients with increased perioperative bleeding
1092 risks, intracranial structural abnormalities, a poor understanding of German or English language, and
1093 patients suffering from postoperative complications. This study was in agreement with the
1094 Declaration of Helsinki and was approved by the Medical Ethical Committee of Charité University
1095 Medicine (record number EA2 127 19). We described patient characteristics of our included
1096 population in Supplementary Table 1.

1097 *Surgical protocol and invasive neural recordings*

1098 Standard clinical care subthalamic electrode implantations took place according to stereotactic gold
1099 standard procedures. All patients received Medtronic SenSight electrodes (Medtronic ©,
1100 Minneapolis, MI, US), except one patient who received Boston Scientific Cartesia X (Boston Scientific
1101 ©, Marlborough, MA, US) electrodes. 13 out of 21 patients agreed to be implanted with an additional
1102 unilateral electrocorticography (ECoG) electrode containing 6 linearly arranged contacts (Ad-tech
1103 Medical Instrument ©, Oak Creek, WI, US). To minimalize additional perioperative risks, the ECoG-
1104 electrode implantation took place at the intraoperative second hemisphere. To minimize cardiac
1105 artefacts during future chronic sensing with implanted internal pulse generators [102], the majority of
1106 ECoG-electrodes was implanted over the right hemisphere. All recordings took place in between the
1107 first surgery for DBS electrodes implantation and the second surgery for internal pulse generator
1108 (IPG) implantation. Details on implanted neural recording hardware is summarized in Supplementary
1109 Table 2.

1110 *Cortical, subthalamic, and kinematic recordings*

1111 Neural and kinematic recordings were sampled via one amplifier (TMSi SAGA, TMSi International,
1112 Oldenzaal, The Netherlands) with a sampling frequency of 4000 Hz. All subthalamic and cortical local
1113 field potential (LFP) recordings had a bipolar configuration, using the lowest subthalamic ring-contact
1114 contralateral to the ECoG-electrode as a common reference. In case of no ECoG-electrode implanted,
1115 the lowest subthalamic ring-contact ipsilateral to the most affected body side was used as a common
1116 reference. A patch-electrode on the right shoulder was used as a ground-electrode. We recorded
1117 kinematic data using two tri-axial accelerometers, one attached to the distal end of each index finger.
1118 We videotaped all recordings continuously to for blinded post hoc clinical assessments.

1119 *Behavioral protocol and clinical assessments*

1120 Patients started the experimental protocol in the "OFF"-condition, deprived from dopamine for at
1121 least 12 hours. At virtual time point zero, they took 1,5 times their dopaminergic morning dosage
1122 (100 to 300 milligrams) as fast-acting L-Dopa (Madopar LT, Roche ©, Basel, CH) (Table S1).
1123 The participants showed the first clinical signs of LID after 21.0 minutes on average (sd: 15.5
1124 minutes). Five out of eighteen subjects that developed LID showed some first, i.e., transient,
1125 dyskinetic signs within 5 minutes after levodopa-intake. The remaining thirteen subjects had an
1126 average LID onset of 29.0 minutes (sd: 10.0 minutes). The three participants that did not develop LID
1127 received higher preoperative levodopa equivalent daily dosages (LEDD) (1873 milligrams (mg), sd:
1128 534 mg, versus 1084 mg, sd: 455 mg, $p = 0.039$, Mann-Whitney-U (mwu)), and received higher
1129 experimental dopaminergic doses (250 mg, sd: 40 mg, versus 179 mg, sd: 39 mg, $p = 0.037$). This
1130 comparison is limited by unbalanced group sizes. The eighteen patients that did develop LID had

mean peak dyskinesia severities of 5 CDRS points (sd: 3, range: 2 to 13 CDRS points), out of a maximum of 28 points (the latter corresponds to severe dyskinetic movement in all seven rated body parts).
The patients started with a 3 to 5 minutes rest recording at the beginning of the experiment around levodopa intake, which was repeated 2 to 4 times throughout the protocol. In between the seated rest recordings, the patients performed a self-paced hand tap task. Data collection continued for 60 – 75 minutes after levodopa intake and unscripted pauses were incorporated to avoid experiment abortion due to exhaustion of the patient. Data collection was continued during the unscripted pauses. During the rest recordings, we instructed the patients to sit still with opened-eyes and not talk. During the self-paced hand-tap tasks, patients remained seated and got the instruction to raise one hand and tap it one their upper leg. We instructed the patients to self-pace their taps roughly every ten seconds, without internally counting seconds. When patients paused for shorter than 7 seconds, or longer than 12 seconds in-between taps, we corrected their tapping pace.

We performed a UPDRS III assessment before levodopa intake and at the end of the recording. We collected preoperative UPDRS III scores in the dopaminergic OFF- and ON-conditions from preoperative DBS evaluations. The presence and severity of dyskinesia was assessed using the Clinical Dyskinesia Rating Scale (CDRS) throughout the whole experiment based on the video recordings [46]. CDRS scores were assessed every five minutes, to account for fluctuations in LID severity. We chose the CDRS as clinical dyskinesia assessment based on its differentiation between LID in the upper and low extremities, and between the left and right body side. An experienced movement disorders specialist (PK) independently rated all CDRS scores, while being blinded for clinical information and neural data. To categorize LID severities in mild, moderate, and severe, we applied thresholds at 4 and 8 CDRS points. These thresholds were decided upon based on the clinical expert's opinion after being familiar with the CDRS distribution and its correlation with clinical severity of LID.

Kinematic signal processing and movement selection

Accelerometer time series were band passed filtered between 1 and 48 Hz (Finite Impulse Response (FIR) filter with a hamming-window) and notch filtered (FIR, notch width 4 Hz and transition width 10 Hz) to remove line noise. We down sampled accelerometer time series to 512 Hz. The filtered accelerometer signals were transformed into signal vectors magnitudes (svm) according to standard accelerometer practices [103]. A custom movement detection was applied which combined the presence of activity and identified acceleration-peaks to categorize the accelerometer data into movement presence and movement absence. The incorporation of acceleration peaks within this categorization, helped to identify ongoing movements. Based on the variation within the svms, thresholds for movement detection were defined at 0.1 mG (milli-gravity, G: 9.8 m/s^2) and 0.5 mG for respectively ongoing movement and acceleration peaks. The performance of this method was controlled with individual visualizations of detected movements over the course of the experiments (Figure S1 panel C and D). After confirming that the movement selection was successful for all individual subjects, the resulting time stamps of single movement start- and end-points were extracted. These time points were applied to 1) calculate the amount of movement presence within each ten-second window of neural data (as applied in the analysis showed in Figure 7), and 2) to isolate moments of movement presence and movement absence from the ten-second windows. Neural data belonging to movement presence and movement absence moments were merged separately, allowing for the neurophysiological comparison between movement presence and movement absence, as used for the analyses showed in Figures 4 and 5.

Neural signal processing

We band pass filtered all raw multi-channel subthalamic and cortical neural time series, recorded respectively from the STN DBS electrodes and the ECoG electrodes, between 2 and 198 Hz using a FIR bandpass-filter with a hamming-window. A notch filter (FIR, notch width 4 Hz and transition width 10 Hz) removed line noise of 50 Hz including its harmonics. A threshold at eight standard deviations automatically detected segments as artefacts and visual inspections of all recordings confirmed the absence of artefacts after signal cleaning. Down sampling ensured a common sampling frequency of 2048 Hz in all neural time series.

All data were split in ten-second windows with a 50% overlap. We discarded windows with more than 33% of missing data. To reduce the data-dimensionality of the multi-channel neural recordings in an unbiased, data-driven manner, and to increase spectral signal to noise ratios, we applied the spatial-spectral-decomposition (SSD) method. One SSD transformation was calculated per frequency band of interest, on every ten-second window, including all neural channels from one neural recording source (either one STN-, or ECoG-electrode) using the Modular EEg Toolkit (https://github.com/neurophysics/meet) [47]. SSD transforms multi-channel time series into a number of independent, singular component time series optimized for variation within a specified frequency band and uses a singular value decomposition. We selected the first SSD-component per frequency band, which holds the maximum variance within the frequency band of interest. The defined frequency bands of interest are theta (4 – 8 Hz), alpha (8 – 12 Hz), low-beta (12 – 20 Hz), high-beta (20 – 35 Hz), and gamma (60 –90 Hz). We limited the gamma range to 60 and 90 Hz based on previous literature on dyskinesia-related neurophysiological findings [39,41,76]. We divided the selected gamma-band in three SSDs (resp. 60 – 70, 70 – 80, and 80 – 90 Hz), to prevent too large loss of broad-band activity based on the optimization based on an individual narrow gamma peak. The SSD-formula internally normalizes the resulting time series to the power in the neighboring frequencies (defined as 'flanks'). To generalize this normalization step and to improve comparability of SSD results over different frequency ranges of interest, we defined the flank-frequencies for every SSD formula up to 2 Hz and 198 Hz. The only exception are the three gamma-sub-bands that were calculated with identical flank ranges between 2 and 60 Hz, and 90 and 98 Hz.
The windowing and SSD transformations resulted in ten-second windows with one optimized neural time series per frequency range of interest (delta, alpha, low-beta, high-beta, and gamma-I, -II, and -III).

Descriptive spectral analysis

Power spectral densities (PSD) were calculated with a one-second window and a 1 Hz frequency resolution using a welch time-frequency decomposition (applying a Hahn-window and a 50% segment-overlap). Only the powers within the frequency range of interest were extracted for every time series resulting from the SSD transformations (e.g., low-beta (12 – 20 Hz) time series generated the spectral power per 1-Hz bin between 12 and 20 Hz). Finally, we combined the results of all SSD time series to create a full spectrum PSD from 4 to 35 Hz and from 60 to 90 Hz, as visualized in Figures 2 and 3. To allow for inter-individual comparison and group-level analysis, we baseline corrected all spectral powers as the percentage change with respect to the OFF-condition. Using a baseline correction compared to the OFF-condition, the spectral powers contained the same temporal relevance throughout the protocol, which would be lost when a relative spectral power for each time point was calculated. Baseline corrections were performed per 1-Hz bin.
To classify spectral power changes based on the presence and severity of clinically observed LID, we labeled every ten-second window to the nearest CDRS-assessment available. Since CDRS assessments were performed every 3 to 5 minutes, to maximal distance between a spectral power value and a

CDRS assessments was 1.5 to 2.5 minutes. Sum CDRS scores including all bilateral and axial items were included, except for the lateralization analysis. The latter made use of unilateral sums of both body side, excluding the axial CDRS parts in the lateralized LID score.
Squared coherence was applied as a functional connectivity metric [52]. Similar to the spectral power calculation, we applied Welch's methods for PSD and cross-spectral density (CSD) calculation in the formula 2. Squared coherence values were calculated between the two bilateral STNs, and the ipsilateral STN and cortex, composed from the SSD-time series and baseline corrected similarly to the spectral power values.

$$\mathrm{COHsquared} = \left|\mathrm{csd}_{source1\ x\ source2}\right|^2 / (\mathrm{psd}_{\mathrm{source-1}} * \mathrm{psd}_{\mathrm{source-2}})$$

Formula 2: Squared coherence calculation.

Feature extraction and predictive modeling

To extract neural features for the predictive analyses, we used the SSD'd ten-second windows and calculated mean spectral power and spectral variation per frequency range of interest. Spectral powers were calculated using a Welch's decomposition with a Hanning window and one second segments with 50% overlap. Spectral variation was calculated as the coefficient of variation of the envelope of the filtered time series (Hilbert transformation). Since SSD calculations were performed for three sub-bands of broadband gamma within 60 to 90 Hz, we included the maximum value of the three ranges as gamma value. In feature sets including subthalamic data, we included mean values of coherences between the bilateral STNs. In the cortico-subthalamic feature sets we included coherences between the ipsilateral STN and ECoG-recordings. Mean coherences values were calculated for each band width of interest using the respectively SSD'd time series, per ten-second windows.
This feature extraction resulted in individual data sets containing one value per feature for every ten-second window. Every ten-second window was labeled with the nearest dyskinesia assessment.

For the predictive analyses, we applied two different classification models, i.e., a linear model and a neural network leveraging latency embedding strategies [48]. Both models decoded binary LID presence (0: non-dyskinetic states, 1: dyskinetic states) based on the above described features. STN models included local subthalamic features and subthalamic-subthalamic coherences. ECoG models included cortical features. STN-ECoG model included both local subthalamic and cortical features, as well as subthalamic-subthalamic and cortico-subthalamic coherences. A leave one subject out cross-validation was applied for all available subjects. For head-to-head model comparisons, only subjects with an ECoG-electrode (n=13) were included (Figure 8B). For the remaining classifiers (Panel C-E) all available subjects were included (n=21). First, we applied a linear model that decoded LID presence. For this, a ridge-regularized class-weight balanced logistic regression model, implemented in scikit-learn [104] (L-BFGS solver, 100 iterations) was applied. In addition to linear decoding, we utilized non-linear deep learning for classifying binary dyskinesia presence. We used the recently presented CEBRA package (Consistent Embeddings of high-dimensional recordings using auxiliary variables) [48]. The CEBRA contrastive learning method was implemented using the "offset10-model", a five-layer convolutional neural network implemented in PyTorch [105]. The first layer consists of 32 hidden units, followed by three convolutional skip layers, each with 32 hidden units, and a final four-dimensional convolutional output layer. The skip layers created a bottleneck in the temporal filter dimension, reducing it from 10 to 3 samples. A Gaussian Error Linear Unit (GELU) activation function was applied to each layer, with normalization on the output layer. The model used the "constant" temperature

mode, a learning rate of 0.001, and was trained for 1000 iterations with a batch size of 300. Contrastive learning sampling was performed with the InfoNCE loss function [106], using a cosine distance between samples, by selecting time samples within a "time_offset" of 10, along with samples corresponding to the auxiliary dyskinesia binary training target variable. The four-dimensional embedding was following by training a ridge-regularized class-weight balanced logistic regression model, implemented in scikit-learn [104] (L-BFGS solver, 100 iterations), which was also applied for the non-cebra linear classifiers.

Analysis software

We performed all analysis with custom-written code in Python in which we made use of standard libraries as numpy [107], pandas [108], scipy [109], sklearn. The custom libraries tmsi-python-interface [110], meet [111] were used for specific parts of signal processing as referred to in the methods.

Code availability

The full code used for the processing of neural and kinematic data, performing descriptive and predictive analyses, and plotting is available on online: https://github.com/jgvhabets/dyskinesia_neurophys.

Data availability

Data can be made available in anonymized form on reasonable request.

References

102. Neumann, W.-J. *et al.* The sensitivity of ECG contamination to surgical implantation site in brain computer interfaces. *Brain Stimulat.* **14**, 1301–1306 (2021).
103. Habets, J. G. V. *et al.* A First Methodological Development and Validation of ReTap: An Open-Source UPDRS Finger Tapping Assessment Tool Based on Accelerometer-Data. *Sensors* **23**, 5238 (2023).
104. Pedregosa, F. *et al.* Scikit-learn: Machine learning in Python. *J. Mach. Learn. Res.* **12**, 2825–2830 (2011).
105. Paszke, A. *et al.* PyTorch: An Imperative Style, High-Performance Deep Learning Library. Preprint at https://doi.org/10.48550/arXiv.1912.01703 (2019).
106. Oord, A. van den, Li, Y. & Vinyals, O. Representation Learning with Contrastive Predictive Coding. Preprint at https://doi.org/10.48550/arXiv.1807.03748 (2019).
107. Walt, S. van der, Colbert, S. C. & Varoquaux, G. The NumPy Array: A Structure for Efficient Numerical Computation. *Comput. Sci. Eng.* **13**, 22–30 (2011).
108. Reback, W. M., jbrockmendel, Joris Van den Bossche, Tom Augspurger, Phillip Cloud, …. Martin Winkel Jeff. Pandas 1.1.1. https://doi.org/10.5281/zenodo.3993412 (2020).
109. The SciPy Project. SciPy.
110. TMSi International. tmsi-python-interface.
111. Waterstraat, G. Modular EEg Toolkit.